Specialization of the Chromatin Remodeler RSC to Mobilize Partially-Unwrapped Nucleosomes

Alisha Schlichter*, Margaret M. Kasten*, Timothy J. Parnell, and Bradley R. Cairns

Howard Hughes Medical Institute (HHMI), Department of Oncological Sciences, Huntsman Cancer Institute, University of Utah School of Medicine, Salt Lake City, Utah, USA.

For correspondence: brad.cairns@hci.utah.edu.

*These authors contributed equally.

Abstract

SWI/SNF-family chromatin remodeling complexes, such as *S. cerevisiae* RSC, slide and eject nucleosomes to regulate transcription. Within nucleosomes, stiff DNA sequences confer spontaneous partial unwrapping, prompting whether and how SWI/SNF-family remodelers are specialized to remodel partially-unwrapped nucleosomes. *RSC1* and *RSC2* are orthologs of mammalian *PBRM1* (polybromo) which define two separate RSC sub-complexes. Remarkably, *in vitro* the Rsc1-containing complex remodels partially-unwrapped nucleosomes much better than does the Rsc2-containing complex. Moreover, a *rsc1*Δ mutation, but not *rsc2*Δ, is lethal with histone mutations that confer partial unwrapping. Rsc1/2 isoforms both cooperate with the DNA-binding proteins Rsc3/30 and the HMG protein, Hmo1, to remodel partially-unwrapped nucleosomes, but show differential reliance on these factors. Notably, genetic impairment of these factors strongly reduces the expression of genes with wide nucleosome-deficient regions (e.g. ribosomal protein genes), known to harbor partially-unwrapped nucleosomes. Taken together, Rsc1/2 isoforms are specialized through composition and interactions to manage and remodel partially-unwrapped nucleosomes.

19 # Introduction

20

21 Nucleosomes regulate transcription in diverse ways and can either block or attract transcriptional
22 regulators (Workman and Kingston 1998). At promoters, nucleosome positioning and/or occupancy
23 plays a central role in regulating transcription factor binding, with transitions in nucleosome positioning
24 typically accompanying activation. SWI/SNF-family ATP-dependent chromatin remodeling complexes
25 (CRCs) have evolved to conduct nucleosome sliding and ejection, and enable transcription factor access
26 to DNA. These CRCs are complex in both composition and mechanism; they utilize a catalytic ATPase to
27 translocate DNA around nucleosomes to conduct nucleosome sliding and eviction, and contain an
28 additional set of proteins to help target and regulate each complex (Clapier and Cairns 2009, Lorch and
29 Kornberg 2017, Narlikar, Sundaramoorthy, and Owen-Hughes 2013).

30 The SWI/SNF-family remodeler, RSC (Remodels the Structure of Chromatin), from the budding yeast *S.*
31 *cerevisiae,* is both essential and abundant, and has long served as a prototype CRC. RSC complex (like
32 others in the SWI/SNF family) is found in more than one compositional subtype, and contains either
33 Rsc1 or its highly-related paralog, Rsc2 (Cairns et al. 1999). Rsc1 and Rsc2 are orthologs of the
34 mammalian polybromo, as both contain multiple bromodomains, a bromodomain-adjacent homology
35 (BAH) domain, and a DNA binding motif (AT Hook or HMG box). Additional RSC compositional variation
36 has been suggested, involving the association of two additional RSC subunits, Rsc3 and Rsc30
37 (Campsteijn, Wijnands-Collin, and Logie 2007, Chambers et al. 2012), which are zinc cluster DNA-binding
38 proteins with affinity for GC-rich sequences (Badis et al. 2008). *RSC1* and *RSC2* are redundant for
39 viability (*rsc1*Δ *rsc2*Δ mutants are inviable), however loss of only one confers mild but dissimilar
40 phenotypes, suggesting overlapping essential functions alongside limited unique functions (Baetz et al.
41 2004, Chambers et al. 2012, Cairns et al. 1999, Bungard, Reed, and Winter 2004). To gain further
42 understanding regarding the roles of RSC1 and RSC2 complexes, we characterized Rsc1- and Rsc2-
43 containing complexes through purification and *in vitro* biochemical assays, alongside *in vivo* genetic and
44 genomic characterization. Both approaches converged to reveal an interplay of functional roles for
45 Rsc1/2, Rsc3/30 and a partner high-mobility group (HMG) domain protein, Hmo1, in managing partially-
46 unwrapped nucleosomes.

47 Partially-unwrapped nucleosomes are defined here as those in which the DNA has released (or displays
48 a tendency to release) from the histone octamer at one or both of the symmetric locations where DNA
49 enters/exits the nucleosome, while the central DNA gyre maintains association with the octamer. DNA

50 sequences differ in their affinity for histone octamers and propensity to form nucleosomes (Anderson,
51 Thastrom, and Widom 2002); stiff homopolymer AT tracts deter nucleosome formation (Segal and
52 Widom 2009) whereas those with short (5 bp) alternating AT and GC tracts more easily adopt
53 nucleosomal curvature, providing a lower cost in energy for nucleosome formation. The commonly used
54 '601' nucleosome positioning sequence is synthetic, was selected for high affinity (Lowary and Widom
55 1998), and displays a 5 bp AT/GC alternating pattern. In contrast, the *5S* rRNA gene sequence is
56 naturally occurring, of lesser affinity (comparable to genome averages), and the entry/exit DNA displays
57 higher rates of detachment from the octamer – displaying partial unwrapping (Polach and Widom 1995,
58 Dong, Hansen, and van Holde 1990, Li and Widom 2004, Zhou and Gaullier 2019).

59 Prior work has revealed the presence of partially-unwrapped 'fragile' nucleosomes at promoters with an
60 especially wide nucleosome deficient region (NDR), and co-incidence of RSC, including at the majority of
61 ribosomal protein genes (RPGs) (Kubik et al. 2015, Brahma and Henikoff 2019, Knight et al. 2014).
62 Indeed, *in silico* size fractionation of RSC-bound nucleosomes provides evidence that RSC occupies
63 wrapped nucleosomes at the +1 and -1 promoter positions, as well as a partially-unwrapped
64 nucleosome interposed between those two displaying lower/fractional occupancy – the basis for the
65 appearance of a large NDR (Brahma and Henikoff 2019). As partially-unwrapped nucleosomes are likely
66 conformationally diverse (Bilokapic, Strauss, and Halic 2018), RSC may have evolved to both recognize
67 and remodel these nucleosomes. Prior work with the Rsc2-containing form of RSC revealed deficiencies
68 in remodeling partially-unwrapped (H3 R40A) nucleosomes (Somers and Owen-Hughes 2009), further
69 questioning whether an alternative form of RSC might better manage them. RSC mobilization of
70 partially-unwrapped nucleosomes may allow sets of transcription factors regulated access to a section
71 of DNA without keeping the region constitutively nucleosome-free – which may provide regulatory
72 benefits and help maintain genome stability (see Discussion). Here, we provide multiple lines of
73 evidence that a set of proteins in RSC (Rsc1, Rsc3/30), and interacting with RSC (Hmo1), cooperate to
74 help remodel partially-unwrapped nucleosomes *in vitro* and *in vivo*.

75

76 # Results

77

78 **The Rsc3/30 heterodimer preferentially associates with the RSC1 complex via the CT2 domain**

79 Rsc1 and Rsc2 are highly similar proteins (45% identical, 62% similar), with high homology present in the
80 bromodomains, BAH domain, and the CT1 region – whereas the CT2 region, which is required for Rsc1 or
81 Rsc2 assembly into RSC, is considerably more divergent (Cairns et al. 1999). We began by exploring
82 whether these Rsc1- or Rsc2-containing subtypes differ in composition, beyond Rsc1/2 themselves. To
83 determine, we purified RSC sub-complexes using a TAP tag (Puig et al. 2001) on either Rsc1 or Rsc2,
84 which revealed Rsc3/30 at apparent stoichiometric levels in the Rsc1-containing complex, but
85 substoichiometric levels in the Rsc2-containing complex (**Figure 1A, 1B**) (Chambers et al. 2012).
86 Furthermore, when purifications were conducted under increasing salt conditions, Rsc3/30 association
87 with Rsc1-TAP was maintained, but was lost with Rsc2-TAP (**Figure 1 – figure supplement 1**) confirming
88 higher avidity of Rsc3/30 for the Rsc1 sub-type.

89 To identify whether a particular region within Rsc1 mediates this preferential association with Rsc3/30,
90 we performed domain swaps between Rsc1 and Rsc2 (**Figure 1C**) and checked for complementation and
91 Rsc3 association. To assess, *TRP1*-marked plasmids containing Rsc1/2 domain-swap derivatives were
92 transformed into a *rsc1*Δ *rsc2*Δ strain containing *RSC1* on a *URA3*-marked plasmid, and
93 complementation was demonstrated by their ability to lose the *URA3*-marked *RSC1* plasmid with 5FOA
94 (**Figure 1D).** Here, co-immunoprecipitation revealed strong Rsc3 association with Rsc1, and with Rsc2
95 derivatives only if they contained the CT2 region of Rsc1 (**Figure 1E**). Conversely, strong Rsc3 association
96 with Rsc1 was lost when Rsc1 contained the CT2 region of Rsc2. Similar approaches involving internal
97 Rsc1/2 deletions and additional swap positions provided further refinement, narrowing the region on
98 Rsc1 responsible for strong Rsc3/30 association to residues 617-777 (**Figure 1 – figure supplement 2A-**
99 **D**).

100 **The RSC1 complex slides *5S* nucleosomes better than the RSC2 complex**

101 Having defined and isolated the four main RSC subtypes (RSC1 or RSC2, +/- Rsc3/30; **Figure 2A**), we then
102 tested for differences in ATPase activity, and remodeling efficiency, by examining nucleosomes of typical
103 wrapping/affinity, such as those formed with the sea urchin *5S* DNA nucleosome positioning sequence
104 (NPS) and recombinant yeast histones. First, all four RSC complexes displayed similar DNA-dependent
105 ATPase activities in typical V_{max} determinations with plasmid DNA (**Figure 2B**). However, major

106 differences were observed with *5S* nucleosomes – RSC1 complex displayed much greater sliding activity
107 than RSC2 (**Figure 2C**). As shown previously for RSC, all sliding activities with RSC1 and RSC2 complexes
108 are ATP dependent ((Cairns et al. 1996) and **Figure 2 – figure supplement 1A**). RSC1 and RSC2
109 complexes both bound *5S* nucleosomes comparably in the absence of ATP (**Figure 2 – figure supplement**
110 **1B**) indicating that their differences in activities occur after the initial engagement of the *5S* nucleosome.
111 Finally, the Rsc3/30 module did not affect their ATPase activities (**Figure 2B**) nor their binding to *5S*
112 nucleosomes (**Figure 2 – figure supplement 1B**); however, in both the RSC1 and RSC2 complexes,
113 Rsc3/30 inclusion moderately inhibited remodeling (**Figure 2C**). Taken together, RSC1 complex displays
114 markedly higher sliding activity on *5S* nucleosomes compared to RSC2 complex.

115 ***rsc1*Δ mutation is lethal in combination with histone mutations that confer partial unwrapping**

116 In principle, a variety of factors might underlie greater remodeling by RSC1 complexes on *5S*
117 nucleosomes. To provide insight into Rsc1/2 differences and to help guide further *in vitro* approaches,
118 we conducted unbiased genetic screens to identify histone mutations that are selectively lethal with
119 *rsc1*Δ or *rsc2*Δ mutations. Here, we utilized an alanine scanning approach in which each of the histone
120 residues is separately mutated to alanine. To implement, we created *rsc1*Δ or *rsc2*Δ deletions
121 (separately) within a 'histone shuffle' strain (*rsc1*Δ or *rsc2*Δ*, h3-h4*Δ [*H3-H4.URA3*]) and combined those
122 with a library encoding all viable histone H3-H4 alanine substitutions on *TRP1*-marked plasmids
123 (Nakanishi et al. 2008). We then assessed viability following enforced loss of the wild-type *H3-H4*
124 plasmid on 5FOA-containing medium. Histone mutations that are lethal with both *rsc1*Δ and *rsc2*Δ, or
125 lethal uniquely with *rsc2*Δ, were found distributed throughout the nucleosome. In striking contrast,
126 those mutations that were lethal specifically with *rsc1*Δ mapped exclusively within the H3 αN helix
127 region – the position where DNA enters/exits the nucleosome (**Table 1, Figure 3A-B**). Furthermore, the
128 specific H3 αN helix mutations obtained in our screen overlap strongly with those reported to increase
129 partial unwrapping using FRET formats (Ferreira et al. 2007), whereas alanine substitutions that did not
130 show a phenotype (P43A, E50A, K56A) had little effect on FRET/unwrapping (**Table 1- table supplement**
131 **1**). These genetic results strongly suggest that synthetic lethality in *rsc1*Δ strains is because RSC2
132 complexes may have more difficulty remodeling partially-unwrapped nucleosomes than RSC1
133 complexes.

134 **Increased Rsc3/30 association with RSC suppresses phenotypes associated with histone αN helix**
135 **mutant combinations**

136 We then explored whether the genetic differences observed with histone αN helix mutations in
137 combination with *rsc1*Δ or *rsc2*Δ involve differential interaction of Rsc1/2 with Rsc3/30. First, we tested
138 whether the CT2 domain of Rsc1, which interacts better with Rsc3/30 than its counterpart in Rsc2, could
139 confer growth when placed within a Rsc2 derivative. Here, growth was clearly restored to *rsc1*Δ H3
140 G44A and *rsc1*Δ H3 R40A combinations with a plasmid encoding Rsc1 or Rsc2 bearing the Rsc1 CT2, but
141 not with Rsc2 or Rsc1 bearing the Rsc2 CT2 (**Figure 3C**). Additional domain swap experiments localize
142 this complementation to the Rsc3/30 association region in Rsc1 (aa 617-777) (**Figure 3 – figure**
143 **supplement 1A**). As a complementary approach, we tested for *RSC3* or *RSC30* high-copy plasmid
144 suppression. While high-copy *RSC3* or *RSC30* could not rescue *rsc1*Δ αN helix histone combined lethality
145 (data not shown), suppression of the strong temperature sensitivity (Ts^-) phenotype of *rsc1*Δ H3 V46A
146 was observed (**Figure 3D**). Taken together, improving the association/functionality of Rsc3/30
147 suppresses phenotypes associated with αN helix histone mutations – further linking Rsc1/2 and Rsc3/30
148 to partial nucleosome unwrapping.

149 **Rsc1/2 uniqueness is largely independent of bromodomain-histone interactions**

150 We then tested the alternative hypothesis that the bromodomains of Rsc1/2 might interact differently
151 with the main acetylated histone residue within/near the αN helix, H3 K56. However, the H3 K56A
152 mutation was not lethal in combination with either *rsc1*Δ or *rsc2*Δ (**Figure 3A**). We then further tested
153 H3 K56Q, which mimics the acetylated form. The K56Q mutation confers synthetic lethality when
154 combined with *rsc1*Δ, but not with *rsc2*Δ (**Figure 3 – figure supplement 1B**). Furthermore, domain
155 swaps involving the highly homologous bromodomains and BAH domains between Rsc1 and Rsc2 did
156 not confer phenotypic differences, nor did these swaps alter the synthetic lethality of *rsc1*Δ with histone
157 αN helix mutations (**Figure 3 – figure supplement 1A**). Notably, H3 K56A has little effect on DNA
158 unwrapping, whereas K56Q promotes unwrapping (Ferreira et al. 2007) – and is lethal with *rsc1*Δ,
159 further supporting an unwrapping function as being responsible for the phenotype. Thus, the lethality
160 with *rsc1*Δ does not appear linked to bromodomains or histone acetylation.

161 **RSC2 complexes are deficient in remodeling partially-unwrapped nucleosomes**

162 Our genetic results prompted the examination of sliding by the RSC1 and RSC2 complexes on *5S*
163 nucleosomes bearing a mutation (e.g., H3 R40A) that confers partial unwrapping. Although sliding of
164 nucleosomes bearing H3 R40A by either form of RSC is reduced relative to wild-type (WT) *5S*
165 nucleosomes, RSC1 complexes were markedly more active than RSC2 complexes (**Figure 3E**), reinforcing

166 the difference between RSC1 and RSC2. Additionally, both RSC1 and RSC2 complexes bind H3 αN helix
167 mutant *5S* nucleosomes similarly (**Figure 3 – figure supplement 2**), demonstrating that initial
168 nucleosome binding is not inhibited by this octamer mutation, suggesting downstream remodeling
169 activity as the affected step. To better define the extent of partial unwrapping observed on the 174 bp
170 *5S* nucleosome, we conducted ExoIII-S1 nuclease mapping (which removes DNA that is either outside of,
171 or not well wrapped in a nucleosome (Flaus 2011), and combined this with a high-throughput
172 sequencing approach to define the endpoints and proportion of the nuclease-protected species. We
173 found WT 174 bp *5S* nucleosomes display a fully-wrapped side (position 158), and a side of partial
174 unwrapping. Here, WT nucleosomes displayed a much higher proportion of largely-wrapped species
175 (≥135bp) than did H3 R40A nucleosomes **(Figure 3 – figure supplement 3**). Since RSC2 is more deficient
176 than RSC1 in repositioning H3 R40A nucleosomes, the mapping supports the hypothesis that RSC1
177 complexes manage partially-unwrapped nucleosomes better than RSC2 complexes. We note that H3
178 R40A *5S* nucleosomes likely have a distinct conformation that is not distinguished in our nuclease
179 protection assay, since remodeling by both RSC1 and (more so) by RSC2 complexes is inhibited by the H3
180 αN helix mutation (compare Figure 3E with Figure 2C). These mutant octamers may enforce a greater
181 degree of openness or distance between the *5S* DNA ends, as demonstrated previously (Ferreira et al.
182 2007), and thereby inhibit RSC activity – a perturbation better managed by RSC1 complexes.

183 **RSC cooperates with Hmo1 to remodel partially-unwrapped nucleosomes**

184 Hmo1 is an HMGB family protein that stabilizes fragile/partially-unwrapped nucleosomes, particularly at
185 rRNA and ribosomal protein gene promoters (Hall, Wade, and Struhl 2006, Panday and Grove 2017), and
186 thus might cooperate with RSC1 or RSC2 to promote remodeling. We first tested for *rsc/hmo1* genetic
187 interactions by combining *rsc1*Δ or *rsc2*Δ with *hmo1*Δ. Notably, we observe synthetic phenotypes in
188 *rsc1*Δ *hmo1*Δ mutants, but not *rsc2*Δ *hmo1*Δ mutants (**Figure 4A**), suggesting a greater reliance of Rsc2
189 on Hmo1 for functional cooperativity. Furthermore, as we saw with the H3 αN helix mutations, this
190 synthetic sickness was partially complemented by the presence of the Rsc1 CT2, and partially
191 suppressed by high-copy *RSC3* or *RSC30*, providing further support that these proteins work together in
192 a modular manner (**Figure 4B**).

193 To test RSC-Hmo1 associations *in vivo*, we performed co-immunoprecipitations between Rsc1 and Rsc2
194 with Hmo1. Hmo1 was endogenously tagged at its C-terminus with a V5 epitope in Myc-tagged Rsc1 and
195 Rsc2 strains. Here, crosslinked chromatin extracts were prepared from log phase cells and sonicated to
196 primarily mononucleosomes. Immunoprecipitation with anti-Myc or anti-V5 antibody followed by

197 immunoblot analysis revealed that both Rsc1 and Rsc2 co-immunoprecipitate with Hmo1, which
198 represents either a direct interaction between Hmo1 and RSC or colocalization on the same
199 nucleosome(s) (**Figure 4C)**. Taken together, Hmo1 shows physical interaction with Rsc1 and Rsc2, but
200 strong functional/genetic interaction primarily with Rsc2 (RSC2 complexes are reliant on Hmo1, in a
201 *rsc1*Δ strain).

202 **Hmo1 stimulates the sliding activity of Rsc1, and especially Rsc2**

203 Hmo1 stimulates the sliding activity of RSC and SWI/SNF complex *in vitro* on 601 nucleosomes (Hepp et
204 al. 2014), but it is not known whether stimulation applies equally to RSC1 and RSC2 complexes, or has a
205 differential effect on their action upon partially-unwrapped nucleosomes. One explanation for why
206 *rsc1*Δ *hmo1*Δ mutants grow more poorly than *rsc2*Δ *hmo1*Δ mutants is that RSC1 is able to remodel
207 those locations in the absence of Hmo1, but RSC2 is not. As Hmo1 enhances RSC remodeling activity
208 (Hepp et al. 2014), we preincubated the *5S* nucleosomal template with increasing amounts of purified
209 Hmo1 and tested for stimulation of RSC1/2 sliding activity. Interestingly, Hmo1 moderately stimulates
210 RSC1 activity, whereas Hmo1 greatly stimulates RSC2 activity (**Figure 4D**), a property that is even more
211 evident in conditions of limiting remodeler or at early time points (**Figure 4 – figure supplement 1**).
212 Moreover, both RSC1 and RSC2 slide the *5S* nucleosome at lower remodeler concentrations in the
213 presence of Hmo1 (30 nM RSC without Hmo1 compare with 10 nM RSC with Hmo1), further supporting
214 a role for Hmo1 in stimulating RSC remodeling activity.

215 **Well-wrapped nucleosomes are remodeled comparably by both RSC1 and RSC2 complexes**

216 Beyond Hmo1 addition, we explored the ability of RSC1 and RSC2 complexes to remodel nucleosomes
217 bearing a very strong positioning sequence: the optimized 601 sequence. Here, RSC1 and RSC2
218 complexes both displayed robust sliding activity with 601 nucleosomes, with RSC1 activity slightly higher
219 (**Figure 4E**). We note a correlation here and in prior work (Clapier et al. 2016) between ejection and the
220 use of strong positioning sequences, – their initial stability from favored 'phasing' may convert to high
221 instability and disfavored 'phasing' after 5 bp of DNA translocation – which may underlie the progressive
222 ejection observed with 601 nucleosomes.

223 We then explored whether an extremely strong positioning sequence (601) might remain wrapped in
224 the presence of an αN helix mutation and rescue RSC2 remodeling. Indeed, we found robust
225 remodeling of 601 H3 R40A nucleosomes by RSC2 (**Figure 4- figure supplement 2A)**, and (by nuclease
226 susceptibility) found that these nucleosomes remain largely wrapped (**Figure 4- figure supplement 2B**).

227 Our data supports the model that while the H3 R40A mutation can result in an open and more loosely
228 wrapped nucleosome conformation, this can be overcome by a strong DNA positioning sequence. In
229 addition, the data shows that the αN helix H3 R40A mutation itself does not impair remodeling by RSC2
230 unless that mutation confers partial unwrapping due to the underlying DNA sequence.

231 **Rsc1 and Rsc2 occupy wide NDRs, with Rsc1 specifically occupying tDNAs**

232 RSC has been examined by chromatin co-immunoprecipitation (ChIP) in several formats (Damelin et al.
233 2002, Yen et al. 2012, Vinayachandran et al. 2018, Brahma and Henikoff 2019), though only one study
234 has examined Rsc1/2 differences. This early ChIP approach with microarrays examined Rsc1 and Rsc2
235 differences, and revealed similar promoter targets for RSC1 and RSC2 complexes (Ng et al. 2002).
236 However, possible issues of sensitivity with earlier data combined with the ability to perform more
237 advanced approaches and analyses prompted ChIP-seq experiments to reveal possible differences.
238 Recent examination of Sth1/RSC occupancy by the 'cut and run' MNase approach (which would have
239 superimposed and not distinguished between Rsc1 and Rsc2 occupancy) revealed general enrichment
240 for RSC complexes at many +1 and -1 nucleosomes, as well as high enrichment of RSC within the NDR of
241 genes with very wide NDRs (e.g., ribosomal protein genes). Notably, these wide NDR regions/promoters
242 have been shown to contain RSC bound to partially-unwrapped nucleosomes, rather than complete lack
243 nucleosomes (Brahma and Henikoff 2019). Therefore, we will hereafter refer to them as 'partially-
244 unwrapped regions' when appropriate, and use the term 'NDR' to generally refer to the nucleosome-
245 deficient regions between the -1 and +1 nucleosome.

246 To further examine the genome-wide location of RSC1 and RSC2 complexes, and their relation to
247 nucleosome wrapping, we utilized MYC-tagged derivatives of Rsc1, Rsc2 and Rsc3 (tagged at their
248 endogenous loci) and performed MNase-based ChIP-seq from logarithmically growing cells. We observe
249 RSC at locations similar to prior work (Brahma and Henikoff 2019), and largely comparable profiles
250 between Rsc1 and Rsc2 at most Pol II genes (as described previously (Ng et al. 2002)). However, we
251 observe interesting features in two regions: promoters with wide NDRs and tDNAs.

252 First, we observed high occupancy of RSC (Rsc1, Rsc2 and Rsc3; **Figure 5A**) at promoters with wide NDRs,
253 with Rsc1 appearing slightly more enriched than Rsc2. As promoters with partially-unwrapped
254 nucleosomes often contain the HMGB protein, Hmo1, we also compared the occupancy of Hmo1 using
255 the ChIP-seq data (Knight et al, 2014) reprocessed using our parameters. Notably, Hmo1 occupancy
256 positively correlates with regions displaying the widest NDRs and bearing the highest Rsc1 and Rsc2

257 occupancy, with an apparent higher correlation with Rsc1 (**Figure 5A-D**). The loci with the highest Hmo1
258 occupancy displayed a mean region size of 336 bp, and a remarkable two-thirds of those genes were
259 ribosomal protein genes (RPGs). Ribosomal protein gene promoters contain GC-rich sequences within
260 their 'NDR' region, and in keeping, we observe Rsc3 enrichment, consistent with Rsc3/30 involvement in
261 targeting or retention.

262 The most striking difference between Rsc1 and Rsc2 occupancy was observed at tDNAs. tDNAs encode
263 tRNAs, and they are among the most nucleosome-depleted loci in the yeast genome, due at least in part
264 to the action of RSC (Parnell, Huff, and Cairns 2008) and their high fractional occupancy by RNA
265 polymerase III transcription factors (Kumar and Bhargava 2013). Here, Rsc1 complexes are markedly
266 more enriched than Rsc2 complexes, and Hmo1 is notably absent (**Figure 5E, F**). The consistent presence
267 of Pol III complexes likely underlies the lack of Hmo1 at tDNAs, as the DNA is not available for binding at
268 tDNAs in the same manner as at a promoter NDR. Taken together, Rsc1 and Rsc2 both highly occupy Pol
269 II promoters known to contain partially-unwrapped nucleosomes and Hmo1, whereas Rsc1 uniquely
270 occupies tDNAs, occupied by Pol III factors.

271 **RSC and HMO1 cooperate to regulate gene expression**

272 To address the transcriptional effects of each of these proteins, we performed RNAseq on
273 logarithmically growing WT, *rsc1*Δ, *rsc2*Δ, *hmo1*Δ, *rsc1*Δ *hmo1*Δ, and *rsc2*Δ *hmo1*Δ cells cultured in SC
274 media. We observe modest differences in transcriptional profiles between WT, *rsc1*Δ, and *rsc2*Δ (**Figure**
275 **5G-H**), which we interpret to be reflective of the known redundancy between Rsc1 and Rsc2 for most
276 functions.

277 However, combining *rsc1*Δ or *rsc2*Δ with *hmo1*Δ resulted in a strong transcriptional shift, resulting in the
278 upregulation (>2-fold) and downregulation (>2-fold) of ~1000 genes (**Figure 5G**), with the most affected
279 class of genes including RPGs, which are downregulated (**Figure 5H**). Additionally the transcriptional shift
280 observed in the double mutants largely mirrors the shift of both up-regulation and down-regulation
281 observed in response to environmental stress response (ESR) genes (Gasch et al. 2000, Brion et al. 2016)
282 (**Figure 5- figure supplement 1).** These results suggest that Rsc1 and Rsc2 both cooperate with Hmo1 to
283 promote the transcription of ribosomal proteins genes, and that the burden for chromatin remodeling
284 at these loci requires the action of both Rsc1 and Rsc2, if Hmo1 is absent.

285 As Rsc3/30 also interact with and affect Rsc1/2 function, we further analyzed *rsc1*Δ *rsc30*Δ, and *rsc2*Δ
286 *rsc30*Δ mutants (**Figure 5- figure supplement 2)**. Remarkably, only *rsc2*Δ *rsc30*Δ mutants impact RP

287 genes – suggesting that the RSC1 complex, which interacts more strongly with Rsc3/30, is more reliant
288 on Rsc3/30 than is RSC2 complex. Taken together, our results are consistent with RSC1 complexes
289 bearing a higher intrinsic ability to mobilize partially-unwrapped nucleosomes compared to RSC2,
290 augmented by partner proteins that preferentially assist either RSC1 (Rsc3/30) or RSC2 (Hmo1)
291 complexes to more efficiently remodel at locations with partially-wrapped nucleosomes (**Figure 6**).

292

293 DISCUSSION

294

295 Genomes are diverse in DNA sequence composition, and the biophysical properties of DNA – in
296 particular, DNA curvature and stiffness – creating a spectrum of affinities for nucleosomes, the main
297 packaging unit of chromatin. This spectrum can undergo selection to create regions where nucleosome
298 formation, positioning, and/or turnover is favored or disfavored, properties which can be utilized at
299 promoters and enhancers to help regulate transcription factor binding, transcription, and ultimately
300 fitness. These biophysical properties work in concert (and sometimes in opposition) with the action of
301 chromatin remodelers, which utilize ATP to move nucleosomes to either favored or disfavored positions,
302 and to eject nucleosomes to provide regulated access of transcription factors to DNA. The commonness
303 in yeast of stiff/disfavored DNA sequences at proximal promoters, juxtaposed to bendable/favorable
304 sequences at the -1 and +1 positions (especially at constitutive or highly transcribed genes), raises the
305 possibility that chromatin remodelers may have undergone specialization to manage the remodeling of
306 both fully wrapped and partially-unwrapped nucleosomes.

307 Here, we provide several lines of evidence that the RSC1 complex can slide partially-unwrapped
308 nucleosomes better than its paralog, the RSC2 complex (**Figure 6**). First, RSC1 acts more efficiently on *5S*
309 nucleosomes, and retains activity on nucleosomes bearing H3 R40A, a mutation that favors unwrapping,
310 whereas RSC2 is relatively impaired. Second, an unbiased genetic screen revealed synthetic lethality
311 with *rsc1*Δ αN helix combinations, but not *rsc2*Δ αN helix combinations, strongly suggesting that the
312 RSC2 complex has more difficulty remodeling partially-unwrapped nucleosomes. Third, Hmo1 stabilizes
313 nucleosomes (Panday and Grove 2016, 2017), and we observe synthetic phenotypes with *rsc1*Δ *hmo1*Δ
314 mutants, but not with *rsc2*Δ *hmo1*Δ mutants (**Figure 4A**), suggesting that Rsc2 relies much more on
315 Hmo1 for functional cooperativity than does Rsc1. This result is paralleled in our remodeling
316 experiments, which show a more pronounced rescue of *5S* nucleosome sliding by RSC2 complexes than

317 RSC1 complexes with recombinant Hmo1 (**Figure 4D**). We note that as nucleosome binding affinity is
318 very similar between RSC1 and RSC2 complexes, the defect/challenge in remodeling with the RSC2
319 complex may involve a step downstream of binding, perhaps involving the ability of the complex to
320 commit to the initiation of DNA translocation, which may be sensitive to the conformation of the
321 nucleosome. Also, nucleosome conformation/wrapping may impact the efficiency of DNA translocation
322 – termed 'coupling' – which involves the probability of each ATP hydrolysis resulting in 1 bp of
323 productive DNA translocation, a property known to be regulated in RSC complex by the actin-related
324 proteins, Arp7 and Arp9 (Clapier et al. 2016, Szerlong et al. 2008).

325 The mammalian polybromo protein (PBRM1) helps define the PBAF sub-complex of mammalian
326 SWI/SNF complex, and is similar in domain composition to the combination of Rsc1/2 and the Rsc4
327 protein (which contains multiple bromodomains). PBRM1 also contains an HMG domain, which is
328 notably absent in the Rsc1, 2, and 4 combination of domains. Here, we speculate that the Hmo1 protein
329 and the HMG domain of PBRM1 may have functional similarities in managing DNA wrapping, which can
330 be tested in future work.

331 RSC contains two proteins with affinity for GC-rich sequences: the paralogs Rsc3 and Rsc30. Here, we
332 reveal a higher avidity of the Rsc3/30 module for the RSC1 complex, localize the region of interaction of
333 Rsc3/30 with Rsc1/2 to the beginning of the CT2 domain, and provide genetic evidence that the
334 preferred interaction of Rsc3/30 with Rsc1 has functional consequences. A current curiosity is the
335 observation – true for both Rsc1 and Rsc2 complexes – that the presence of Rsc3/30 moderately inhibits
336 remodeling, while the genetics supports a positive role for Rsc3/30 in assisting Rsc1/2 function. One
337 obvious role for Rsc3/30 is in targeting RSC to GC-rich sequences such as ribosomal protein genes, which
338 likely underlies the essential nature of Rsc3/30 function. Here, future work may explore whether
339 Rsc3/30 serve a regulatory role in the remodeling reaction, with their modest attenuation function
340 relieved in the proper regulatory contexts of DNA sequence (e.g., GC richness) and protein composition
341 (i.e., Hmo1, others) to help confer environmental sensing and properly regulate RPGs.

342 Given our exploration of Rsc1/2 paralog and Rsc3/30 paralog function, we also explored their evolution
343 (**Figure 5 – figure supplement 3**). A whole genome duplication (WGD) occurred within the
344 *Saccharomyces* lineage approximately 150 million years ago (Wolfe and Shields 1997) resulting in
345 *RSC1/2* paralogs. We find the single *RSC1/2* ortholog present in species that did not undergo the WGD
346 (e.g. *Zygosaccharomyces, Ashbya*, and *Lachancea*), more closely related to *RSC2* than *RSC1*, suggesting
347 *RSC2* as the more ancient ortholog (**Figure 5- table supplement 1)**. Interestingly, species more distant to

348 *S. cerevisae* lack both *RSC3* and *RSC30*. Following the appearance of *RSC3*, the WGD event then created
349 *RSC1/2* and *RSC3/RSC30* orthologs, along with duplications of the ribosomal protein genes, a large
350 fraction of which have been maintained in *Saccharomyces cerevisiae*. Finally, *HMO1* predates the
351 appearance of *RSC3* and the WGD. Thus, specialization of Rsc1 to preferentially bind Rsc3/30 and play a
352 role in the regulation of the ribosomal protein genes was enabled by the WGD, and may have arisen to
353 help rapidly and properly regulate RPGs in response to growth conditions.

354 In favorable growth conditions, approximately 50% of the transcriptional effort of RNA Pol II is directed
355 at RPGs (Warner 1999). Our work supports and greatly extends the prior work of others (Knight et al.
356 2014, Hepp et al. 2017, Wade, Hall, and Struhl 2004) that *S. cerevisiae* has evolved many ways to 'poise'
357 chromatin at RPG promoters in a relatively 'open and ready' format. These promoters have evolved to
358 be less favorable to nucleosomes by bearing regions of 'stiff' AT-rich DNA (Segal and Widom 2009)
359 (note: Rsc1/2 each bear an AT hook), are punctuated by GC-rich DNA (known Rsc3/30 binding sites), and
360 use histone acetylation (e.g. H3 K56ac) (Neumann et al. 2009), Hmo1 (Hall, Wade, and K. Struhl, 2006),
361 DNA-binding general regulatory factors (e.g. Rap1, Abf1) and chromatin remodeling complexes such as
362 RSC and SWI/SNF complex – that together help keep these regions nucleosome deficient and partially-
363 unwrapped (Kubik et al. 2018, Hepp et al. 2017, Brahma and Henikoff 2019, Reja et al. 2015). While
364 RSC1 and RSC2 complexes appear largely redundant at most genes, and can both be assisted at RPG
365 promoters by Hmo1, our work supports the notion that the RSC1 complex, through its ability to better
366 manage partially-unwrapped nucleosomes and preferential association with Rsc3/30, has become
367 specialized to help perform this role (**Figure 6**). This combination of specialization and partial
368 redundancy provides this system the needed robustness and the ability to conduct rapid and
369 sophisticated activation/regulation of this important RPG class – attributes which may contribute to
370 fitness in diverse environments.

371

372 # MATERIALS AND METHODS

373

374 **Strains, Media, Yeast growth, and Assay Replication**

375 Rich media (YPD), synthetic complete (SC), and sporulation media were prepared using standard
376 methods. Standard procedures were used for transformations, sporulation, tetrad analysis and spotting.
377 A null mutation of Hmo1 was obtained from Invitrogen and crossed into *rsc1* and *rsc2* deletion strains.
378 Rsc1 was C-terminally TAP-tagged as described by (Rigaut et al. 1999), and Hmo1 C-terminally tagged
379 with V5 as described in (Funakoshi and Hochstrasser 2009). Full genotypes of yeast strains are available
380 in **Supplementary File 1**. A technical replicate is defined as a test of the same sample multiple times,
381 whereas a biological replicate is defined as the same test run on multiple biological samples of
382 independent origin. The number and type of replicates for each experiment is indicated in the figure
383 legend.

384

385 **Plasmid Construction**

386 DNA encoding Rsc1 w/Rsc2 CT2 was created by PCR amplification of RSC2 CT2 from position K617
387 through the end of the gene, using primers containing 40bp homology to *RSC1* or vector sequence. PCR
388 product was co-transformed with linearized p609 (314.RSC1) into YBC800 (rsc1Δ rsc2Δ [316.RSC1]) and
389 homologous recombination inserted the DNA encoding CT2 into *RSC1* beginning at position K617. Rsc2
390 w/1CT2 at position K656 was created by amplifying *RSC1* CT2 on p609 (314.RSC1) and co-transforming
391 into linearized p604 (314.RSC2) into YBC803 (*rsc1Δ rsc2Δ* [316.RSC2]) and repaired by homologous
392 recombination. Plasmid was isolated from TRP positive colonies, sequenced, and retransformed to check
393 for complementation. Additional swaps were constructed similarly. Internal deletions in Rsc1 and Rsc2
394 were created by digesting with restriction enzymes with blunt or compatible ends, removing the small
395 fragment and ligating ends back together. Plasmid markers were swapped as needed as described in
396 (Cross 1997). A full list of plasmids used in this study is provided in **Supplementary File 2**.

397

398 **RSC1 and RSC2 TAP purification**

399 RSC complexes were purified from *S. cerevisiae* strains BCY211 (RSC2-TAP) and BCY516 (RSC1-TAP)
400 harboring an integrated version of the C-terminally Tandem Affinity Purification (TAP)-tagged on the

401 construct of the indicated gene. Purifications were performed essentially as described (Rigaut et al.
402 1999) (Szerlong et al. 2008) with the following modifications. After harvesting, cells were washed with
403 0.5x PBS + 10% glycerol, pelleted, and frozen in liquid nitrogen as pea-size pieces. Frozen cells were
404 pulverized in a SPEX SamplePrep 6850 Freezer/Mill at a rate of 10, for 10 cycles of 3 min 'on' and 2 min
405 'off', with the resulting powder stored at -80°C until purification.

406 RSC1+3/30 complex was purified from BCY516 essentially as described (Szerlong et al. 2008) with the
407 following modifications since Rsc1 is found at lower levels than Rsc2 in yeast cells. Pulverized cells (160
408 g) were solubilized in Lysis Buffer (50 mM HEPES [pH 7.5], 400 mM KOAc, 10 mM EDTA, 20% glycerol, 0.5
409 mM BME, protease inhibitors). The KOAc concentration of the lysate was brought to 450 mM and
410 nucleic acids were precipitated with 0.1-0.2% polyethyleneimine. The cleared lysate was incubated with
411 5 ml IgG Sepharose 6 Fast Flow (GE Healthcare) for 3 h, the resin sequentially washed with Lysis Buffer,
412 IgG Wash Buffer (20 mM Tris-Cl, [pH 8], 400 mM KOAc, 0.1% Igepal, 1 mM EDTA, 0.5 mM BME, protease
413 inhibitors), and IgG Elution Buffer (20 mM Tris-Cl [pH 8], 200 mM KOAc, 10% glycerol, 0.1% Igepal, 0.5
414 mM BME). The RSC1-TAP complex was cleaved from the IgG resin with 500 U AcTEV enzyme (Invitrogen)
415 gently rotating the slurry at 15°C for 1 h followed by 4°C rotation overnight. The eluate was collected,
416 brought to 3 mM $CaCl_2$, and bound to 1.5 ml Calmodulin Affinity Resin (Agilent Technologies) overnight.
417 The resin was washed with 250 Calmodulin Wash Buffer (20 mM Tris-Cl [pH 7.5], 250 mM NaCl, 1 mM
418 Mg Acetate, 1 mM imidazole, 2 mM CaCl2, 10% glycerol, 0.1% Igepal, 0.5 mM BME, protease inhibitors).
419 The RSC1 complex was eluted with 250 Calmodulin Elution Buffer (20 mM Tris-Cl [pH 7.5], 250 mM NaCl,
420 2 mM EGTA, 10% glycerol, 0.1% Igepal, 0.5 mM BME, protease inhibitors) in successive 500-750 µl
421 fractions. The RSC1-containing fractions were determined, pooled, and residual nucleic acid was
422 removed by a final DEAE Sepharose clean-up step. The complex was concentrated on a Vivaspin 30K PES
423 concentrator, concentration was determined by Bradford assay (Bio-Rad) and confirmed by silver
424 stained polyacrylamide SDS-PAGE analysis.

425 RSC1-3/30 complex was purified as described above except the IgG Wash Buffer had 750 mM NaCl
426 instead of KOAc, and the IgG resin was rotated overnight during the IgG Wash step to remove the
427 Rsc3/30 module. The bound IgG resin was equilibrated into IgG Elution Buffer before cleaving with
428 AcTEV.

429 RSC2+3/30 complex was purified as above with the following modifications. Approximately 80 g of
430 pulverized BCY211 cells were solubilized in Lysis Buffer. Cleared lysates were incubated with IgG
431 Sepharose, washed and eluted with AcTEV enzyme as above. The eluate was collected, brought to 3 mM

432 $CaCl_2$, and bound to 1.5 ml Calmodulin Affinity Resin for 3 h. The resin was washed with 200 KOAc
433 Calmodulin Wash (same as Calmodulin Wash but with 200 mM KOAc replacing the NaCl) followed by
434 150 NaCl Calmodulin Wash (same as Calmodulin Wash but with 150 mM NaCl). The RSC2 complex was
435 eluted with 150 Calmodulin Elution Buffer (same as above but with 150 mM NaCl) in successive 500-750
436 μl fractions. The RSC2-containing fractions were determined and pooled. The salt was increased to 250
437 mM NaCl and residual nucleic acid was removed on DEAE Sepharose. The complex was immediately
438 diluted to 125 mM NaCl while maintaining the other buffer component concentrations. The complex
439 was concentrated and the concentration was determined as above.

440 RSC2-3/30 complex was purified essentially as the RSC2+3/30 complex with the following modifications.
441 After binding the Calmodulin Affinity Resin, the resin was washed with 200 KOAc Calmodulin Wash
442 Buffer, followed by four 20 min washes with 500 mM NaCl Calmodulin Wash Buffer, and a final rinse
443 with 150 NaCl Calmodulin Wash Buffer to equilibrate the resin. The RSC2-3/30 complex was eluted from
444 the Calmodulin Affinity Resin, residual nucleic acid removed on DEAE Sepharose, concentrated and
445 quantified as above for the RSC2+3/30 complex.

446 **Hmo1 Purification**

447 Recombinant Hmo1 was purified from bacteria as an N-terminal fusion to 8xHIS (plasmid from T.
448 Formosa). Briefly, *E. coli* BL21-CodonPlus(DE3)RIL transformed with pET.8xHIS.Hmo1 was induced with
449 IPTG at 30°C for 3 h to express the fusion protein. Cells were harvested, resuspended in HIS Lysis Buffer
450 (20 mM Tris [pH 8], 500 mM NaCl, 10 mM imidazole, 10% glycerol, 0.1% Igepal, 1.5 mM BME, protease
451 inhibitors), and lysed by sonication. The lysate was cleared and bound to pre-equilibrated Ni-NTA
452 agarose beads (Qiagen) for 1.5 h. The bound resin was washed sequentially with HIS tag Lysis Buffer, Ni
453 Wash Buffer A (same as HIS Lysis Buffer but with 30 mM imidazole), and Ni Wash Buffer B (same as HIS
454 Lysis Buffer but with 50 mM imidazole). The protein was eluted with Ni Elution Buffer (20 mM Tris [pH
455 8], 500 mM NaCl, 250 mM imidazole, 10% glycerol, 0.005% Igepal, 1.5 mM BME, protease inhibitors) and
456 sized on a Superdex 200 gel filtration column (GE). Hmo1 ran as a soluble aggregate (approximately 440
457 kD) larger than predicted from its molecular weight (27.5 kD). The Hmo1 protein was dialyzed into 150
458 mM Sizing Buffer (20 mM Tris [pH 8], 150 mM NaCl, 10% glycerol, 1.5 mM BME, protease inhibitors) and
459 concentrated before storing at -80°C in aliquots.

460 **RSC1 and RSC2 Rsc3/30 Stringency Testing**

461 Stringency testing on Rsc3/30 association with RSC1 and RSC2 was conducted on IgG Sepharose. Cells
462 were grown and pulverized as for RSC purification. Sixty grams of RSC1-TAP cells and 20 g of RSC2-TAP
463 cells were solubilized in Lysis Buffer and the lysate was cleared as above. One milliliter of IgG resin was
464 incubated with the cleared lysate for 2 h. The beads were washed with Lysis Buffer, and then with IgG
465 Wash Buffer, before being split into 10 separate Eppendorf tubes for testing. The beads were gently
466 pelleted, rinsed 3 times with the specific IgG Wash Buffer containing 150, 250, or 500 mM NaCl, as
467 indicated. The specific IgG Wash Buffer was added for 1 h or 16 h (overnight), as indicated. All beads
468 were washed 3 times with IgG Elution Buffer, resuspended in IgG Elution Buffer, and RSC was released
469 from the beads with AcTEV enzyme as above and 1/10th of the eluate was analyzed by silver stain on a
470 6% SDS polyacrylamide gel.

471 **Co-Immunoprecipitations**

472 Whole cell extracts were prepared and co-immunoprecipitations for RSC were performed as described,
473 (Cairns et al. 1999) with the following modification. Anti-Myc or anti-HA antibodies (0.6 µg) were bound
474 to a 25 µl slurry of pan-mouse magnetic Dynabeads (Thermo Fisher) and incubated with 1000 µg of
475 extract. Blots were probed with anti-Sth1 (Saha, Wittmeyer, and Cairns 2002), anti-Rsc3, anti-Rsc30
476 (Angus-Hill et al. 2001), anti-Rsc2 and anti-Rsc4 (Kasten et al. 2004).

477 Extracts for Rsc1 and Rsc2 chromatin co-IPs with Hmo1 were prepared from cells grown to OD_{600}= 0.8,
478 Cultures were crosslinked in 1% formaldehyde final for 30min at RT, quenched with 0.2M glycine, and
479 lysed by bead-beating (mini-beadbeater, Biospec) in LB140 buffer. Samples were sonicated in a
480 Bioruptor Pico (Diagenode) to release chromatin. Immunoprecipitations were performed with 1000 µg
481 of extract and a 25 µl slurry of pan-mouse Dynabeads bound to anti-Myc (Abcam) or anti-V5 (Thermo-
482 Fisher) antibodies.

483 **Nucleosome Assembly**

484 Yeast octamers were produced using purified *S. cerevisiae* histones expressed in *E. coli* BL21-
485 CodonPlus(DE3)RIL. Either wild-type histone H3 or the H3 R40A mutant was assembled into yeast
486 octamers by salt-dialysis, essentially as described previously (Dyer et al. 2004). Mononucleosomes were
487 assembled from a linear salt gradient dialysis (2 M to 50 mM KCl) using Slide-A-Lyser Mini Dialysis units
488 with a 7,000 molecular weight cutoff (Thermo Scientific) essentially as described (Clapier et al. 2016)
489 using one of several DNA positioning sequences. The 205 bp Widom 601 positioning sequence (Lowary
490 and Widom 1998) were produced from pUC12x601 digested with AvaI and purified using preparative

491 electrophoresis (PrepCell, Bio-Rad). The 174 bp sea urchin *5S* positioning sequence was prepared by PCR
492 amplification using a plasmid containing a copy of the sea urchin *5S* sequence as a template. The PCR
493 product was precipitated before purifying on a PrepCell. The exact 601 and *5S* positioning sequences
494 used are given in **File Supplement 2**. Assembled mononucleosomes were separated from free DNA by
495 gradient sedimentation on a 10-30% sucrose gradient as previously described (Wittmeyer, Saha, and
496 Cairns 2004).

497 **ATPase Assays**

498 Measurement of ATP hydrolysis was as described previously (Saha, Wittmeyer, and Cairns 2002,
499 Wittmeyer, Saha, and Cairns 2004) using a color (malachite green) absorbance assay that quantitatively
500 measures released free phosphate. Assays were performed on three separate purifications of each type
501 of RSC complex. Reactions were performed in duplicate. Activities were measured at V_{max} using double-
502 stranded Bluescript plasmid as the substrate.

503 **Nucleosome Sliding Assay**

504 Nucleosome sliding assays were performed as described (Clapier et al. 2016) with the following
505 modifications. Reactions were conducted in 10 mM Tris [pH 7.4], 50 mM KCl, 3 mM $MgCl_2$, 0.1 mg/ml
506 BSA, 1 mM ATP with 20 nM mononucleosomes at 30°C and 400 rpm shaking in a Thermomixer
507 (Eppendorf). The amount of remodeler varied. Sliding reactions on 205 bp 601 nucleosomes used 10 nM
508 RSC. Sliding reactions on 174 bp *5S* nucleosomes used 30 nM RSC unless otherwise indicated. Aliquots
509 were removed at each time point and reactions were stopped by adding 10 mM EDTA + 200 ng
510 competitor DNA (Bluescript plasmid). Samples were loaded with 10% glycerol on a 4.5% (37.5:1) native
511 polyacrylamide gel and run in 0.4x TBE for 45 min at 110 V constant. Gels were stained with ethidium
512 bromide solution and scanned on a Typhoon Trio (Amersham, GE).

513 **Nucleosome Gel Shift Assays**

514 Nucleosome gel shift assays were conducted similarly to the nucleosome sliding assay described above
515 with the following modifications. Reactions were conducted in the absence of ATP and at 30°C for 20
516 min with 20 nM mononucleosomes. The RSC remodelers were added at 30 and 60 nM. The reactions
517 were loaded on to 3.8% (37.5:1) native polyacrylamide gels and run in 0.4x TBE for 55 min at 110 V
518 constant without addition of any stop solution or competitor. Gels were stained with ethidium bromide
519 solution and scanned on a Typhoon Trio.

520 **Histone Mutant Screen**

521 Null mutations in *rsc1* and r*sc2* were crossed into the H3/H4 shuffle strain WZY42 (Zhang et al. 1998).
522 Strains YBC1939 (WZY42), YBC2090 and YBC3040 were transformed in 96 well plate format with a TRP-
523 marked histone H3-H4 mutant plasmid library, obtained from and screened as described previously
524 (Nakanishi et al. 2008). Transformants were spotted to SC-TRP plates, replica plated again to SC-TRP
525 plates after 2 days, followed by replica plating to SC-TRP and SC-TRP + 5FOA. Synthetic lethality with
526 mutations in the H3 αN helix were confirmed by a second round of individual transformations and
527 shuffles.

528 **Recombinant Nucleosome Mapping**

529 The position and wrapping of the recombinant nucleosomes were determined by sequencing the
530 protected DNA fragment after treating assembled nucleosomes with Exonuclease III and S1 nuclease.
531 Approximately 400-800 fmol of nucleosomes purified from sucrose gradients was digested with a 5-25U
532 titration of ExoIII enzyme (New England Biolabs) for 1, 2, or 3 min at 37°C in ExoIII Buffer (10 mM Tris
533 [pH 8], 50 mM NaCl, 3 mM $MgCl_2$). Reactions were moved to ice, S1 Buffer and NaCl were added (30 mM
534 NaOAc [pH 4.6], 1 mM ZnOAc, 5% glycerol, and 300 mM NaCl final concentration), and treated with 50U
535 S1 for 30 min at room temperature. Tris [pH 8.8] and EDTA were added to final concentrations of 88 mM
536 and 14 mM, respectively, and heated to 70°C for 10 min. SDS was added to 1%, vortexed, and iced. The
537 protected DNA fragments were cleaned up on a Qiagen MinElute PCR purification column and eluted in
538 30 μl EB. The level of digestion was determined for each sample on a 4.5% (37.5:1) native
539 polyacrylamide 0.4x TBE gel as described above.

540 Libraries were made from the above protected fragments using the NEBNext ChIP-Seq MasterMix Set
541 (New England Biolabs) with the following modifications. Samples did not go through the initial End-
542 Repair. A custom adaptor with an 8 bp unique molecular identifier (UMI) was ligated onto the dA-tailed
543 samples. The UMI Adaptor was created from an oligo based on the standard NEBNext adaptor sequence
544 incorporating 8 random nucleotides at the 5' end of the oligo (see oligo sequence in **File Supplement 2**).
545 To create the UMI Adaptor, 25 μM oligo (synthesized by IDT) was first heated to 95°C and slow cooled
546 to room temperature in Duplex Buffer (100 mM KOAc, 30 mM HEPES [pH 7.5]). The ends of the
547 annealed UMI Adaptor were filled in using Klenow (New England Biolabs). The reaction was stopped
548 with EDTA and heat. The adaptor was cleaned up on a Micro Bio-Spin 6 chromatography column (Bio-
549 Rad) equilibrated with water. A dT-tail was added to the adaptor with Klenow exo- (New England

550 Biolabs). The UMI Adaptor was cleaned up on a Micro Bio-Spin 6 column and eluted in water. The UMI
551 Adaptor was diluted to 1.14 μM final concentration for use in library preparations. High-throughput
552 sequencing was performed by Illumina's protocol for 50 bp paired-end runs on an Illumina HiSeq 2500
553 or a MiSeq.

554 The embedded UMI code was first extracted from the Fastq files using the script
555 embedded_UMI_extractor from the package UMIScripts
556 (https://github.com/HuntsmanCancerInstitute/UMIScripts). Output Fastq sequences were then aligned
557 to an index comprised of the recombinant sea urchin *5S* or 601 sequence using Novocraft Novoalign
558 (version 3.8.2), giving the adapter sequences for trimming. After alignment, PCR-duplicate reads were
559 identified and marked based on the UMI information with the UMISripts application bam_umi_dedup.
560 The 5' start positions for each alignment, discarding duplicates, were recorded as a bigWig file with 1 bp
561 resolution using the application bam2wig from the BioToolBox package
562 (https://github.com/tjparnell/biotoolbox). Separate bigWig files were generated for each length of
563 alignments (92-169 bp). To normalize for sequencing read depth, alignment counts were scaled to an
564 equivalent of 100K reads (calculated from the total sum of alignments without regard to alignment
565 length). Count matrices for each length at each position on the reference sequence and for each sample
566 were then collected using the BioToolBox application get_datasets from the bigWig files. Count matrices
567 were analyzed with Microsoft Excel employing a 5% cutoff of the normalized fragment count.

568

569 **ChIP Seq and Analysis**

570 Yeast cultures from yHN1 (YBC1544-RSC1.9XMYC) and yHN2 (YBC1545; RSC2.9XMYC) (Ng et al. 2002)
571 were grown in SC-TRP at 30°C with two biological replicates. Cultures were harvested at OD_{600}= 0.8, and
572 crosslinked with 1% formaldehyde final for 30 min at room temperature. Cultures were quenched with
573 0.2M glycine for 5 min. Chromatin extracts were prepared by bead-beating, and chromatin was
574 liberated with micrococcal nuclease. Immunoprecipitation was performed using anti-cMyc 9E11
575 (Abcam). DNA was isolated for input and IP samples and assembled into a library using Illumina
576 protocols and sequenced as single end reads on an Illumina sequencer.

577 Fastq sequences were aligned to the yeast genome (UCSC version SacCer3) with NovoCraft Novoalign
578 (version 3.8.2), allowing for one random alignment for multi-mapping reads. To maintain processing
579 consistency between single-end and paired-end alignments, paired-end was aligned as single-end by

580 ignoring the second read. Alignments were processed using the MultiRepMacsChIPSeq pipeline (version
581 10.1, https://github.com/HuntsmanCancerInstitute/MultiRepMacsChIPSeq). Since MNase-digested
582 chromatin yields high levels of coordinate-duplicate alignments (observed mean of 65%, range 57% to
583 74%), duplicate alignments were randomly subsampled to a uniform rate of 40% to remove sample bias
584 while retaining relative signal intensity. Alignments over ribosomal DNA, telomeric sequences,
585 mitochondrial chromosome, and other high copy sequences were excluded. Fragment coverage tracks
586 were generated by extending alignments in the 3' direction by 160 bp in all fragments. We note that
587 there may be some between-sample biases in the distribution of MNase-digested fragment lengths,
588 particularly with RSC-enriched fragments, but rationalized that uniformity of processing should help
589 minimize these biases. Replicates were depth-normalized (Reads Per Million) prior to combining as an
590 average after confirming reasonable similarity to each through standard correlation metrics. Log2 fold
591 enrichment of ChIP signal over non-enriched nucleosome signal (Input) was generated with Macs2
592 (Zhang et al. 2008) without background lambda correction. Hmo1 ChIPs (GSM1509041) (Knight et al.
593 2014) were re-processed in a similar manner.

594 NDRs were determined by first determining all nucleosome positions in the genome using the software
595 package biotoolbox-nucleosome (https://github.com/tjparnell/biotoolbox-nucleosome) with the Input
596 MNase sample alignments. To reduce mapping noise and increase efficacy of calling positions, "skinny"
597 nucleosome coverage was used rather than midpoint data. Fragment coverage was generated by
598 shifting the 5' alignment coordinate in the 3' direction by 37 bp and extending 74 bp, essentially
599 recording the predicted central portion of the nucleosome. After mapping nucleosomes, NDRs were
600 extracted by calculating all inter-nucleosomal intervals and selecting for those with lengths between 75
601 and 600 bp and occurring over or adjacent to a defined protein-coding gene TSS. NDRs were sorted by
602 decreasing length and aligned by the edge closest to the TSS; NDRs between divergent promoter pairs
603 are represented once.

604 Data was collected with applications from the BioToolBox package
605 (https://github.com/tjparnell/biotoolbox). Mean occupancy of RSC and Hmo1 were collected over the
606 NDRs using the application get_datasets, while spatial data surrounding NDRs and tDNAs were collected
607 with get_relative_data. Heat maps were generated in R (R Core Team 2018) with pHeatmap (Kolde
608 2019). Dot plots and violin plots were generated with GraphPad Prism.

609 **RNA seq and Analysis**

610 Yeast cultures for RNASeq were grown in SD media supplemented for auxotrophic amino acids at 30°C in
611 three biological replicates. RNA from logarithmically growing cells was purified using Ambion Ribo-pure
612 yeast kit. Samples were additionally DNAse-treated and cleaned up with Qiagen RNeasy kit. Illumina
613 Ribo Zero yeast kit was used for library preparation, and sequencing performed on an Illumina
614 sequencer.

615 Fastq reads were processed following an RNASeq pipeline
616 (https://github.com/HuntsmanCancerInstitute/hciR). Briefly, reads were aligned with STAR (version
617 2.5.4, (Dobin et al. 2013), counts obtained with Subread featureCounts (version 1.6.3) based on Ensembl
618 annotation (release 90), and differential gene expression performed with DESeq2 (version 1.21). Dot
619 plots and violin plots were generated with GraphPad Prism (version 8.0.2).

620

621 **Acknowledgements:**

We thank Brian Dalley and the High-Throughput Sequencing Shared Resource for sequencing data. We thank Ali Shilatifard, Tim Formosa, Jef Boeke, Kevin Struhl, Anne Grove, Roger Kornberg and Sharon Dent for strains and plasmids. We thank Patrick Murphy and Edward Grow for helpful discussions on data analysis and experimental design and Naveen Verma for feedback on the manuscript. We thank HHMI for support of A.S, M.K and B.C, and thank NCI CA042014 to Huntsman Cancer Institute for support of core facilities. A.S., M.K., and B.C. designed the project. A.S. and M.K. conducted the experiments and prepared the figures. T.P. provided genomics analysis and genomics figures. B.C. wrote the manuscript with contributions from all authors.

Competing Interests

None of the authors have competing financial or non-financial interests related to the work in this manuscript.

622 **Supplemental Information**

623 Figure 1- figure supplement 1. The Rsc3/30 module associates with the Rsc1 complex at high stringency.

624 Figure 1- figure supplement 2. Additional swaps and truncations define the region of Rsc3/30
625 association.
626 Figure 2- figure supplement 1. RSC complexes without Rsc3/30 module are ATP-dependent chromatin
627 remodelers and RSC1 and RSC2 complexes bind similarly to 174b bp sea urchin *5S* mononucleosomes.
628 Table Supplement 1. DNA end to end FRET measurement on mononucleosomes containing H3 αN helix
629 mutations with the phenotype when combined with *rsc1*Δ, *rsc2*Δ.
630 Figure 3- figure supplement 1. Complementation by CT2 domain swaps when combined with H3 αN
631 helix mutations.
632 Figure 3- figure supplement 2. RSC1 and RSC2 complexes bind similarly to 174bp sea urchin
633 mononucleosomes with the H3 R40A mutation.
634 Figure 4- figure supplement 1. Additional sliding assays of 174bp *5S* yeast mononucleosomes pre-
635 incubated with increasing concentrations of Hmo1.
636 Figure 4- figure supplement 2. RSC1 and RSC2 complexes slide Widom 601 H3 R40A mononucleosomes
637 similarly.
638 Figure 5- figure supplement 1. Gene expression changes in *rsc1*Δ, *rsc2*Δ, and *hmo1*Δ mutants.
639 Figure 5- figure supplement 2. Gene expression changes in *rsc1*Δ, *rsc2*Δ, and *rsc30*Δ mutants.
640 Figure 5- figure supplement 3. Appearance of *RSC1/RSC2*, *RSC3/RSC30* and *HMO1* orthologs in yeast
641 evolution.
642 Figure 5- table Supplement 1. Alignment scores from NCBI fungal BLAST for Rsc1/Rsc2 and Rsc3/30
643 orthologs.
644 Supplementary File 1. Table of yeast strains and their genotypes used in this study.
645 Supplementary File 2. Table of plasmids and DNA sequences used in this study.
646 Figure 3- figure supplement 3- Source data 1. 174bp *5S* nucleosome mapping.
647 Figure 4- figure supplement 2- Source data 1. 205 bp Widom 601 nucleosome mapping.
648 Figure 5- Source data 1- Files for generation of occupancy heat maps.
649 Figure 5- Source data 2- RSC occupancy at promoters and tDNAs.
650 Figure 5- Source data 3- Differential gene expression.
651 Figure 5- figure supplement 1- Source data 1- List of ESR affected genes.
652
653 Raw sequencing data is available at NCBI under SRA accession number PRJNA573112.
654

655 # References

656

657 Anderson, J. D., A. Thastrom, and J. Widom. 2002. "Spontaneous access of proteins to buried
658 nucleosomal DNA target sites occurs via a mechanism that is distinct from nucleosome
659 translocation." *Molecular and Cellular Biology* 22 (20):7147-7157. doi:
660 10.1128/Mcb.22.20.7147-7157.2002.

661 Angus-Hill, M. L., A. Schlichter, D. Roberts, H. Erdjument-Bromage, P. Tempst, and B. R. Cairns. 2001. "A
662 Rsc3/Rsc30 zinc cluster dimer reveals novel roles for the chromatin remodeler RSC in gene
663 expression and cell cycle control." *Mol Cell* 7 (4):741-51. doi: 10.1016/S1097-2765(01)00219-2.

664 Badis, G., E. T. Chan, H. van Bakel, L. Pena-Castillo, D. Tillo, K. Tsui, C. D. Carlson, A. J. Gossett, M. J.
665 Hasinoff, C. L. Warren, M. Gebbia, S. Talukder, A. Yang, S. Mnaimneh, D. Terterov, D. Coburn, A.
666 Li Yeo, Z. X. Yeo, N. D. Clarke, J. D. Lieb, A. Z. Ansari, C. Nislow, and T. R. Hughes. 2008. "A library
667 of yeast transcription factor motifs reveals a widespread function for Rsc3 in targeting
668 nucleosome exclusion at promoters." *Mol Cell* 32 (6):878-87. doi:
669 10.1016/j.molcel.2008.11.020.

670 Baetz, K. K., N. J. Krogan, A. Emili, J. Greenblatt, and P. Hieter. 2004. "The ctf13-30/CTF13 genomic
671 haploinsufficiency modifier screen identifies the yeast chromatin remodeling complex RSC,
672 which is required for the establishment of sister chromatid cohesion." *Mol Cell Biol* 24 (3):1232-
673 44. doi: 10.1128/mcb.24.3.1232-1244.2003.

674 Bilokapic, S., M. Strauss, and M. Halic. 2018. "Histone octamer rearranges to adapt to DNA unwrapping."
675 *Nat Struct Mol Biol* 25 (1):101-108. doi: 10.1038/s41594-017-0005-5.

676 Brahma, S., and S. Henikoff. 2019. "RSC-Associated Subnucleosomes Define MNase-Sensitive Promoters
677 in Yeast." *Mol Cell* 73 (2):238-249.e3. doi: 10.1016/j.molcel.2018.10.046.

678 Brion, C., D. Pflieger, S. Souali-Crespo, A. Friedrich, and J. Schacherer. 2016. "Differences in
679 environmental stress response among yeasts is consistent with species-specific lifestyles." *Mol
680 Biol Cell* 27 (10):1694-705. doi: 10.1091/mbc.E15-12-0816.

681 Bungard, D., M. Reed, and E. Winter. 2004. "RSC1 and RSC2 are required for expression of mid-late
682 sporulation-specific genes in Saccharomyces cerevisiae." *Eukaryot Cell* 3 (4):910-8. doi:
683 10.1128/ec.3.4.910-918.2004.

684 Cairns, B. R., Y. Lorch, Y. Li, M. Zhang, L. Lacomis, H. Erdjument-Bromage, P. Tempst, J. Du, B. Laurent,
685 and R. D. Kornberg. 1996. "RSC, an essential, abundant chromatin-remodeling complex." *Cell* 87
686 (7):1249-60. doi: 10.1016/s0092-8674(00)81820-6.
687 Cairns, B. R., A. Schlichter, H. Erdjument-Bromage, P. Tempst, R. D. Kornberg, and F. Winston. 1999.
688 "Two functionally distinct forms of the RSC nucleosome-remodeling complex, containing
689 essential AT hook, BAH, and bromodomains." *Molecular Cell* 4 (5):715-723. doi: Doi
690 10.1016/S1097-2765(00)80382-2.
691 Campsteijn, C., A. M. Wijnands-Collin, and C. Logie. 2007. "Reverse genetic analysis of the yeast RSC
692 chromatin remodeler reveals a role for RSC3 and SNF5 homolog 1 in ploidy maintenance." *PLoS*
693 *Genet* 3 (6):e92. doi: 10.1371/journal.pgen.0030092.
694 Chambers, A. L., P. M. Brownlee, S. C. Durley, T. Beacham, N. A. Kent, and J. A. Downs. 2012. "The two
695 different isoforms of the RSC chromatin remodeling complex play distinct roles in DNA damage
696 responses." *PLoS One* 7 (2):e32016. doi: 10.1371/journal.pone.0032016.
697 Clapier, C. R., and B. R. Cairns. 2009. "The biology of chromatin remodeling complexes." *Annu Rev*
698 *Biochem* 78:273-304. doi: 10.1146/annurev.biochem.77.062706.153223.
699 Clapier, C. R., M. M. Kasten, T. J. Parnell, R. Viswanathan, H. Szerlong, G. Sirinakis, Y. Zhang, and B. R.
700 Cairns. 2016. "Regulation of DNA Translocation Efficiency within the Chromatin Remodeler
701 RSC/Sth1 Potentiates Nucleosome Sliding and Ejection." *Mol Cell* 62 (3):453-461. doi:
702 10.1016/j.molcel.2016.03.032.
703 Cross, F. R. 1997. "'Marker swap' plasmids: convenient tools for budding yeast molecular genetics."
704 *Yeast* 13 (7):647-53. doi: 10.1002/(SICI)1097-0061(19970615)13:7<647::AID-YEA115>3.0.CO;2-#.
705 Damelin, M., I. Simon, T. I. Moy, B. Wilson, S. Komili, P. Tempst, F. P. Roth, R. A. Young, B. R. Cairns, and
706 P. A. Silver. 2002. "The genome-wide localization of Rsc9, a component of the RSC chromatin-
707 remodeling complex, changes in response to stress." *Mol Cell* 9 (3):563-73. doi: 10.1016/S1097-
708 2765(02)00475-6.
709 Dobin, A., C. A. Davis, F. Schlesinger, J. Drenkow, C. Zaleski, S. Jha, P. Batut, M. Chaisson, and T. R.
710 Gingeras. 2013. "STAR: ultrafast universal RNA-seq aligner." *Bioinformatics* 29 (1):15-21. doi:
711 10.1093/bioinformatics/bts635.
712 Dong, F., J. C. Hansen, and K. E. van Holde. 1990. "DNA and protein determinants of nucleosome
713 positioning on sea urchin 5S rRNA gene sequences in vitro." *Proc Natl Acad Sci U S A* 87
714 (15):5724-8. doi: 10.1073/pnas.87.15.5724.

715 Dyer, P. N., R. S. Edayathumangalam, C. L. White, Y. Bao, S. Chakravarthy, U. M. Muthurajan, and K.
716 Luger. 2004. "Reconstitution of nucleosome core particles from recombinant histones and
717 DNA." *Methods Enzymol* 375:23-44. doi: 10.1016/s0076-6879(03)75002-2.
718 Ferreira, H., J. Somers, R. Webster, A. Flaus, and T. Owen-Hughes. 2007. "Histone tails and the H3
719 alphaN helix regulate nucleosome mobility and stability." *Mol Cell Biol* 27 (11):4037-48. doi:
720 10.1128/mcb.02229-06.
721 Flaus, Andrew. 2011. "Principles and practice of nucleosome positioning in vitro." *Frontiers in Life*
722 *Science* 5 (1-2):5-27. doi: 10.1080/21553769.2012.702667.
723 Funakoshi, M., and M. Hochstrasser. 2009. "Small epitope-linker modules for PCR-based C-terminal
724 tagging in Saccharomyces cerevisiae." *Yeast* 26 (3):185-92. doi: 10.1002/yea.1658.
725 Gasch, A. P., P. T. Spellman, C. M. Kao, O. Carmel-Harel, M. B. Eisen, G. Storz, D. Botstein, and P. O.
726 Brown. 2000. "Genomic expression programs in the response of yeast cells to environmental
727 changes." *Mol Biol Cell* 11 (12):4241-57. doi: 10.1091/mbc.11.12.4241.
728 Hall, D. B., J. T. Wade, and K. Struhl. 2006. "An HMG protein, Hmo1, associates with promoters of many
729 ribosomal protein genes and throughout the rRNA gene locus in Saccharomyces cerevisiae."
730 *Mol Cell Biol* 26 (9):3672-9. doi: 10.1128/mcb.26.9.3672-3679.2006.
731 Hepp, M. I., V. Alarcon, A. Dutta, J. L. Workman, and J. L. Gutierrez. 2014. "Nucleosome remodeling by
732 the SWI/SNF complex is enhanced by yeast high mobility group box (HMGB) proteins." *Biochim*
733 *Biophys Acta* 1839 (9):764-72. doi: 10.1016/j.bbagrm.2014.06.014.
734 Hepp, M. I., M. Smolle, C. Gidi, R. Amigo, N. Valenzuela, A. Arriagada, A. Maureira, M. M. Gogol, M.
735 Torrejon, J. L. Workman, and J. L. Gutierrez. 2017. "Role of Nhp6 and Hmo1 in SWI/SNF
736 occupancy and nucleosome landscape at gene regulatory regions." *Biochim Biophys Acta Gene*
737 *Regul Mech* 1860 (3):316-326. doi: 10.1016/j.bbagrm.2017.01.002.
738 Hyland, Edel M., Michael S. Cosgrove, Henrik Molina, Dongxia Wang, Akhilesh Pandey, Robert J. Cottee,
739 and Jef D. Boeke. 2005. "Insights into the role of histone H3 and histone H4 core modifiable
740 residues in Saccharomyces cerevisiae." *Molecular and cellular biology* 25 (22):10060-10070. doi:
741 10.1128/MCB.25.22.10060-10070.2005.
742 Kasten, M., H. Szerlong, H. Erdjument-Bromage, P. Tempst, M. Werner, and B. R. Cairns. 2004. "Tandem
743 bromodomains in the chromatin remodeler RSC recognize acetylated histone H3 Lys14." *Embo j*
744 23 (6):1348-59. doi: 10.1038/sj.emboj.7600143.
745 Knight, B., S. Kubik, B. Ghosh, M. J. Bruzzone, M. Geertz, V. Martin, N. Denervaud, P. Jacquet, B. Ozkan, J.
746 Rougemont, S. J. Maerkl, F. Naef, and D. Shore. 2014. "Two distinct promoter architectures

747 centered on dynamic nucleosomes control ribosomal protein gene transcription." *Genes Dev* 28
748 (15):1695-709. doi: 10.1101/gad.244434.114.
749 Kolde, Raivo. 2019. "Pretty Heatmaps. Available online at https://cran.r-
750 project.org/web/packages/pheatmap/pheatmap.pdf."
751 Kubik, S., M. J. Bruzzone, P. Jacquet, J. L. Falcone, J. Rougemont, and D. Shore. 2015. "Nucleosome
752 Stability Distinguishes Two Different Promoter Types at All Protein-Coding Genes in Yeast." *Mol*
753 *Cell* 60 (3):422-34. doi: 10.1016/j.molcel.2015.10.002.
754 Kubik, S., E. O'Duibhir, W. J. de Jonge, S. Mattarocci, B. Albert, J. L. Falcone, M. J. Bruzzone, F. C. P.
755 Holstege, and D. Shore. 2018. "Sequence-Directed Action of RSC Remodeler and General
756 Regulatory Factors Modulates +1 Nucleosome Position to Facilitate Transcription." *Mol Cell* 71
757 (1):89-102.e5. doi: 10.1016/j.molcel.2018.05.030.
758 Kumar, Y., and P. Bhargava. 2013. "A unique nucleosome arrangement, maintained actively by
759 chromatin remodelers facilitates transcription of yeast tRNA genes." *BMC Genomics* 14:402.
760 doi: 10.1186/1471-2164-14-402.
761 Li, G., and J. Widom. 2004. "Nucleosomes facilitate their own invasion." *Nat Struct Mol Biol* 11 (8):763-
762 9. doi: 10.1038/nsmb801.
763 Lorch, Y., and R. D. Kornberg. 2017. "Chromatin-remodeling for transcription." *Q Rev Biophys* 50:e5. doi:
764 10.1017/s003358351700004x.
765 Lowary, P. T., and J. Widom. 1998. "New DNA sequence rules for high affinity binding to histone octamer
766 and sequence-directed nucleosome positioning." *J Mol Biol* 276 (1):19-42. doi:
767 10.1006/jmbi.1997.1494.
768 Nakanishi, S., B. W. Sanderson, K. M. Delventhal, W. D. Bradford, K. Staehling-Hampton, and A.
769 Shilatifard. 2008. "A comprehensive library of histone mutants identifies nucleosomal residues
770 required for H3K4 methylation." *Nat Struct Mol Biol* 15 (8):881-8. doi: 10.1038/nsmb.1454.
771 Narlikar, G. J., R. Sundaramoorthy, and T. Owen-Hughes. 2013. "Mechanisms and functions of ATP-
772 dependent chromatin-remodeling enzymes." *Cell* 154 (3):490-503. doi:
773 10.1016/j.cell.2013.07.011.
774 Neumann, H., S. M. Hancock, R. Buning, A. Routh, L. Chapman, J. Somers, T. Owen-Hughes, J. van Noort,
775 D. Rhodes, and J. W. Chin. 2009. "A method for genetically installing site-specific acetylation in
776 recombinant histones defines the effects of H3 K56 acetylation." *Mol Cell* 36 (1):153-63. doi:
777 10.1016/j.molcel.2009.07.027.

778 Ng, H. H., F. Robert, R. A. Young, and K. Struhl. 2002. "Genome-wide location and regulated recruitment
779 of the RSC nucleosome-remodeling complex." *Genes Dev* 16 (7):806-19. doi:
780 10.1101/gad.978902.
781 OhÉigeartaigh, Seán, David Armisén, Kevin Byrne, and Kenneth Wolfe. 2011. "Systematic discovery of
782 unannotated genes in 11 yeast species using a database of orthologous genomic segments."
783 *BMC genomics* 12:377. doi: 10.1186/1471-2164-12-377.
784 Panday, A., and A. Grove. 2016. "The high mobility group protein HMO1 functions as a linker histone in
785 yeast." *Epigenetics Chromatin* 9:13. doi: 10.1186/s13072-016-0062-8.
786 Panday, A., and A. Grove. 2017. "Yeast HMO1: Linker Histone Reinvented." *Microbiol Mol Biol Rev* 81
787 (1). doi: 10.1128/mmbr.00037-16.
788 Parnell, T. J., J. T. Huff, and B. R. Cairns. 2008. "RSC regulates nucleosome positioning at Pol II genes and
789 density at Pol III genes." *Embo j* 27 (1):100-10. doi: 10.1038/sj.emboj.7601946.
790 Polach, K. J., and J. Widom. 1995. "Mechanism of protein access to specific DNA sequences in chromatin:
791 a dynamic equilibrium model for gene regulation." *J Mol Biol* 254 (2):130-49. doi:
792 10.1006/jmbi.1995.0606.
793 Puig, O., F. Caspary, G. Rigaut, B. Rutz, E. Bouveret, E. Bragado-Nilsson, M. Wilm, and B. Seraphin. 2001.
794 "The tandem affinity purification (TAP) method: a general procedure of protein complex
795 purification." *Methods* 24 (3):218-29. doi: 10.1006/meth.2001.1183.
796 R Core Team. 2018. "R: A language and environment for statistical computing." R Foundation for
797 Statistical Computing. Available online at https://www.R-project.org/.
798 Reja, R., V. Vinayachandran, S. Ghosh, and B. F. Pugh. 2015. "Molecular mechanisms of ribosomal
799 protein gene coregulation." *Genes Dev* 29 (18):1942-54. doi: 10.1101/gad.268896.115.
800 Rigaut, G., A. Shevchenko, B. Rutz, M. Wilm, M. Mann, and B. Seraphin. 1999. "A generic protein
801 purification method for protein complex characterization and proteome exploration." *Nat
802 Biotechnol* 17 (10):1030-2. doi: 10.1038/13732.
803 Saha, A., J. Wittmeyer, and B. R. Cairns. 2002. "Chromatin remodeling by RSC involves ATP-dependent
804 DNA translocation." *Genes Dev* 16 (16):2120-34. doi: 10.1101/gad.995002.
805 Segal, E., and J. Widom. 2009. "Poly(dA:dT) tracts: major determinants of nucleosome organization."
806 *Curr Opin Struct Biol* 19 (1):65-71. doi: 10.1016/j.sbi.2009.01.004.
807 Somers, J., and T. Owen-Hughes. 2009. "Mutations to the histone H3 alpha N region selectively alter the
808 outcome of ATP-dependent nucleosome-remodelling reactions." *Nucleic Acids Res* 37 (8):2504-
809 13. doi: 10.1093/nar/gkp114.

810 Szerlong, H., K. Hinata, R. Viswanathan, H. Erdjument-Bromage, P. Tempst, and B. R. Cairns. 2008. "The
811 HSA domain binds nuclear actin-related proteins to regulate chromatin-remodeling ATPases."
812 *Nat Struct Mol Biol* 15 (5):469-76. doi: 10.1038/nsmb.1403.
813 Vinayachandran, Vinesh, Rohit Reja, Matthew J. Rossi, Bongsoo Park, Lila Rieber, Chitvan Mittal, Shaun
814 Mahony, and B. Franklin Pugh. 2018. "Widespread and precise reprogramming of yeast protein-
815 genome interactions in response to heat shock." *Genome research* 28 (3):357-366. doi:
816 10.1101/gr.226761.117.
817 Wade, J. T., D. B. Hall, and K. Struhl. 2004. "The transcription factor Ifh1 is a key regulator of yeast
818 ribosomal protein genes." *Nature* 432 (7020):1054-8. doi: 10.1038/nature03175.
819 Warner, J. R. 1999. "The economics of ribosome biosynthesis in yeast." *Trends Biochem Sci* 24 (11):437-
820 40. doi: 10.1016/s0968-0004(99)01460-7.
821 Wittmeyer, J., A. Saha, and B. Cairns. 2004. "DNA translocation and nucleosome remodeling assays by
822 the RSC chromatin remodeling complex." *Methods Enzymol* 377:322-43. doi: 10.1016/S0076-
823 6879(03)77020-7.
824 Wolfe, K. H., and D. C. Shields. 1997. "Molecular evidence for an ancient duplication of the entire yeast
825 genome." *Nature* 387 (6634):708-13. doi: 10.1038/42711.
826 Workman, J. L., and R. E. Kingston. 1998. "Alteration of nucleosome structure as a mechanism of
827 transcriptional regulation." *Annu Rev Biochem* 67:545-79. doi:
828 10.1146/annurev.biochem.67.1.545.
829 Yen, K., V. Vinayachandran, K. Batta, R. T. Koerber, and B. F. Pugh. 2012. "Genome-wide nucleosome
830 specificity and directionality of chromatin remodelers." *Cell* 149 (7):1461-73. doi:
831 10.1016/j.cell.2012.04.036.
832 Zhang, W., J. R. Bone, D. G. Edmondson, B. M. Turner, and S. Y. Roth. 1998. "Essential and redundant
833 functions of histone acetylation revealed by mutation of target lysines and loss of the Gcn5p
834 acetyltransferase." *EMBO J* 17 (11):3155-67. doi: 10.1093/emboj/17.11.3155.
835 Zhang, Y., T. Liu, C. A. Meyer, J. Eeckhoute, D. S. Johnson, B. E. Bernstein, C. Nusbaum, R. M. Myers, M.
836 Brown, W. Li, and X. S. Liu. 2008. "Model-based analysis of ChIP-Seq (MACS)." *Genome Biol* 9
837 (9):R137. doi: 10.1186/gb-2008-9-9-r137.
838 Zhou, K., and G. Gaullier. 2019. "Nucleosome structure and dynamics are coming of age." 26 (1):3-13.
839 doi: 10.1038/s41594-018-0166-x.

840

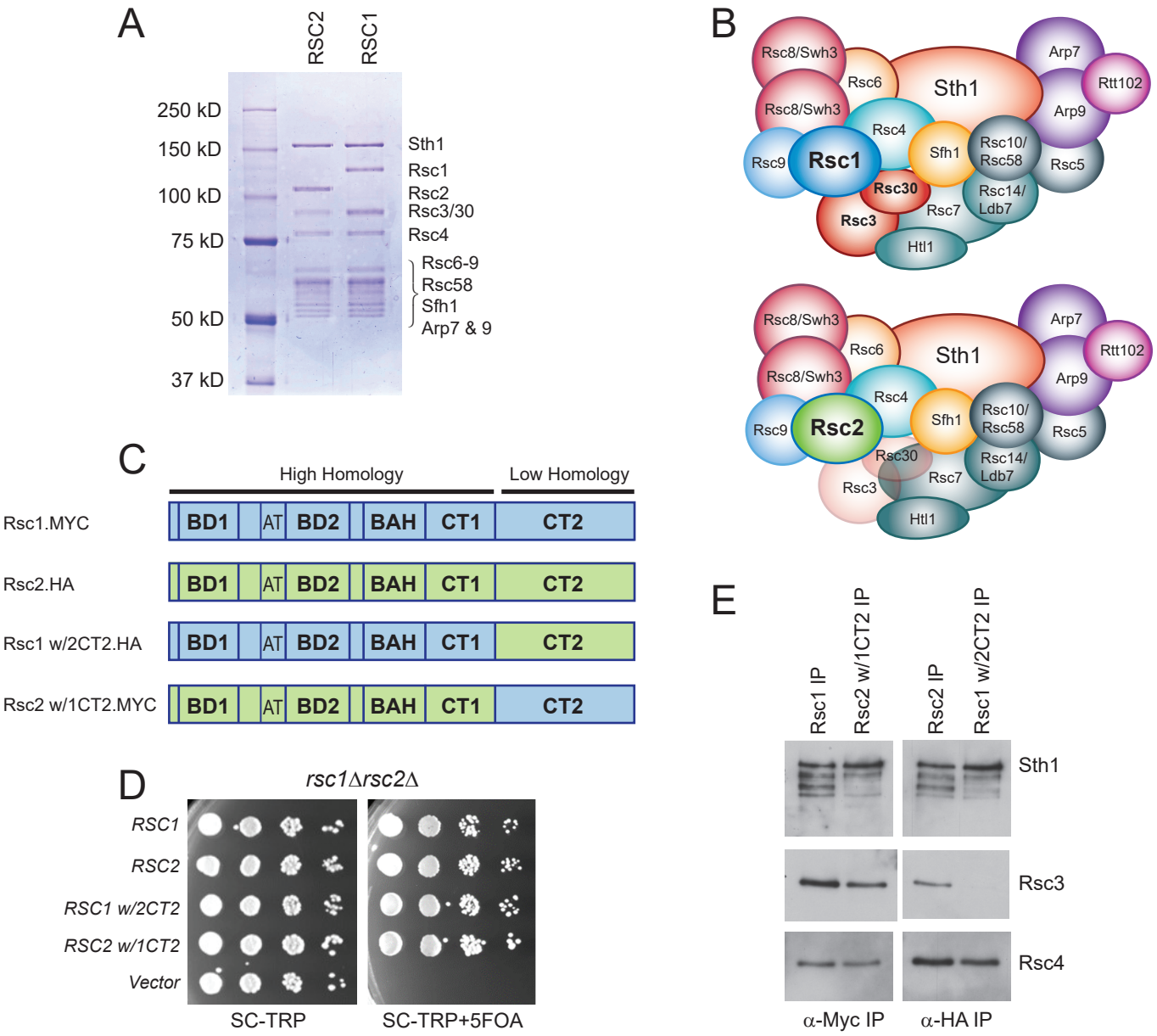

Figure 1. Rsc3/30 module has higher avidity for the RSC1 complex. (A) Purified RSC1-TAP and RSC2-TAP complexes (2 μg) analyzed on 7.5% SDS-PAGE gel stained with Coomassie dye. (B) RSC1 and RSC2 complex compositions, with decreased opacity displaying the reduced association of the Rsc3/30 module in the RSC2 complex. (C) Domain structure and swaps of Rsc1 and Rsc2. (D) CT2 domain swaps complement for viability. *TRP1*-marked plasmids bearing *RSC1* (p609), *RSC2* (p604), *RSC1 w/2CT2* (p3097), *RSC2 w/1CT2* (p3098), or vector (pRS314) were transformed into *rsc1Δrsc2Δ* [*RSC1.URA3*] (YBC800), and spotted as 10x serial dilutions to SC-TRP or to SC-TRP+5FOA to force the loss of the *RSC1.URA3* plasmid. 'w/' indicates 'with'. One of four biological replicates shown. (E) The Rsc3/30 module associates more strongly with the CT2 region of Rsc1. Immunoprecipitations of Rsc1, Rsc2 w/1CT2, Rsc2, Rsc1 w/2CT2 from whole cell extracts. Blots were probed with anti-Sth1, then stripped and reprobed for anti-Rsc3 and anti-Rsc4. One of three technical replicates shown.
Figure 1- figure supplement 1. The Rsc3/30 module associates with the RSC1 complex at high stringency.
Figure 1- figure supplement 2. Additional swaps and truncations define the region of Rsc3/30 association.

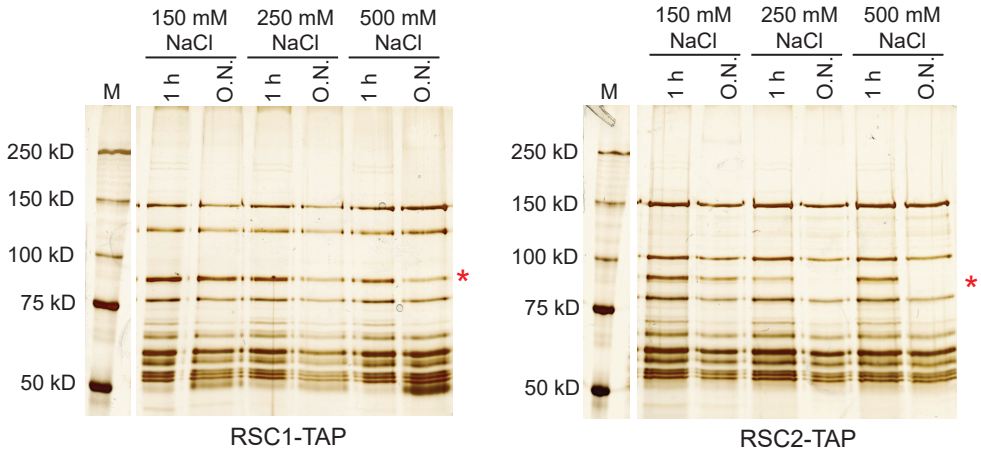

Figure 1 - figure supplement 1. The Rsc3/30 module associates with the RSC1 complex at high stringency. Yeast cell lysates containing RSC-TAP complexes were bound to IgG resin, the beads rinsed with lysis buffer before washing with buffer of the indicated salt concentration and duration. RSC complexes were analyzed on 6% acrylamide SDS-PAGE gels stained with silver. The Rsc3 and Rsc30 proteins run closely on denaturing gels and the doublet will often appear as a single band, marked by the asterisk (*). The marker lanes (M) are each from the adjacent gel, but were moved for depiction. Stringency testing conducted once.

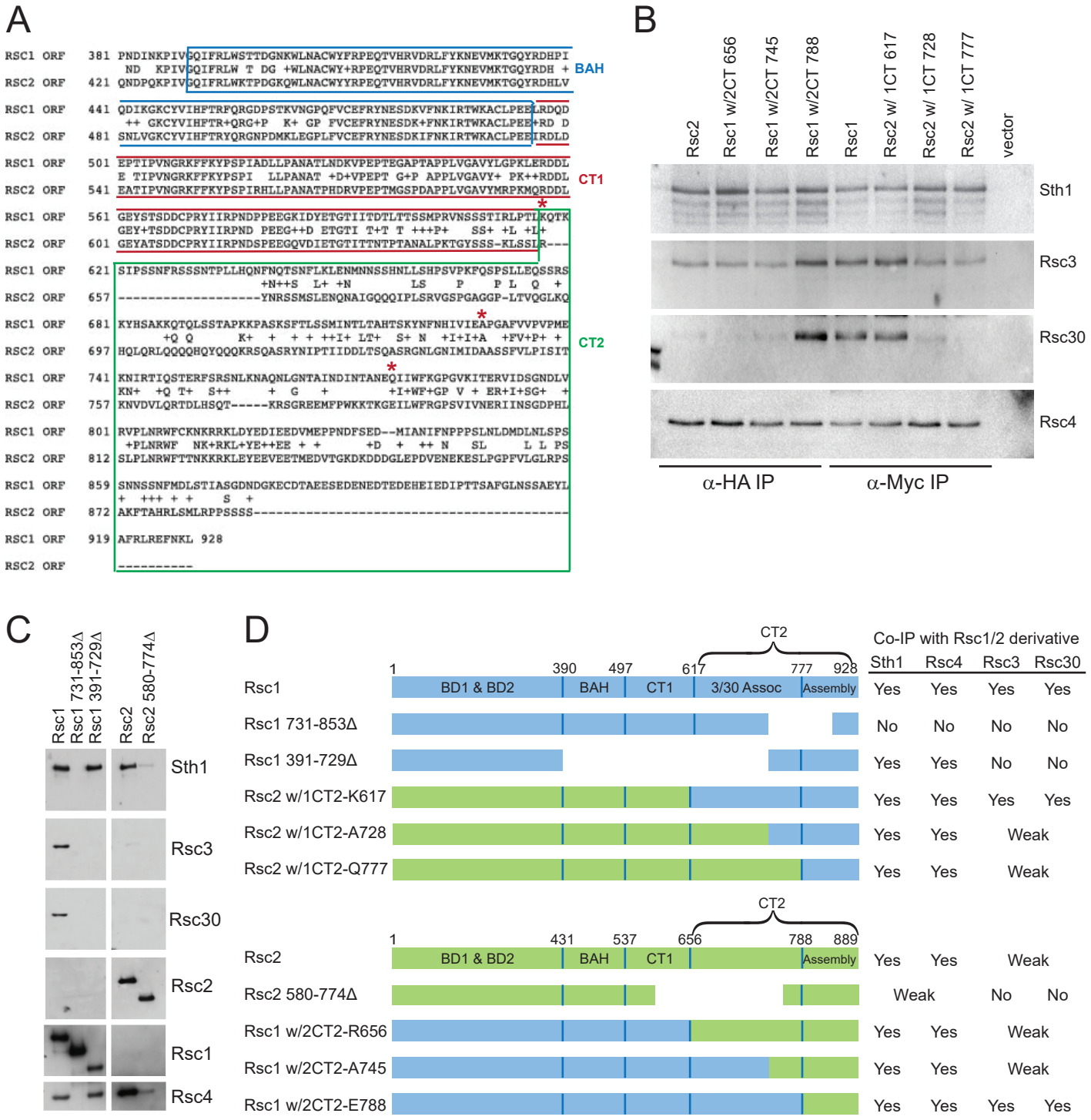

Figure 1 - figure supplement 2. Additional swaps and truncations define the region of Rsc3/30 association. (A) Alignment of C-terminus of Rsc1 and Rsc2, showing conservation and position of swaps (red asterisks). (B) Co-IPs of Rsc3 and Rsc30 with additional Rsc1 and Rsc2 CT swaps. Whole cell extracts prepared from *rsc1Δrsc2Δ* covered by *TRP1*-marked plasmid containing *RSC1*, *RSC2,* or CT swap were immunoprecipitated using anti-Myc (for CT2 of Rsc1), or anti-HA (for CT2 of Rsc2) bound to Dynabeads. Western blots were probed with antibodies against Sth1, Rsc3, Rsc30, and Rsc4. One of three biological replicates shown. (C) Co-IPs of RSC members with Rsc1 or Rsc2 containing deletions within the CT2 region. Whole cell extracts prepared from *rsc1Δrsc2Δ* covered by *TRP1*-marked plasmid containing deletions were immunoprecipitated using anti-Myc (for CT2 of Rsc1), or anti-HA (for CT2 of Rsc2) bound Dynabeads. Western blots were probed with antibodies against Sth1, Rsc3, Rsc30, Rsc2, Rsc4, and Myc. One of three technical replicates shown. (D) Summary of Rsc1 and Rsc2 Co-IPs from deletions and swaps.

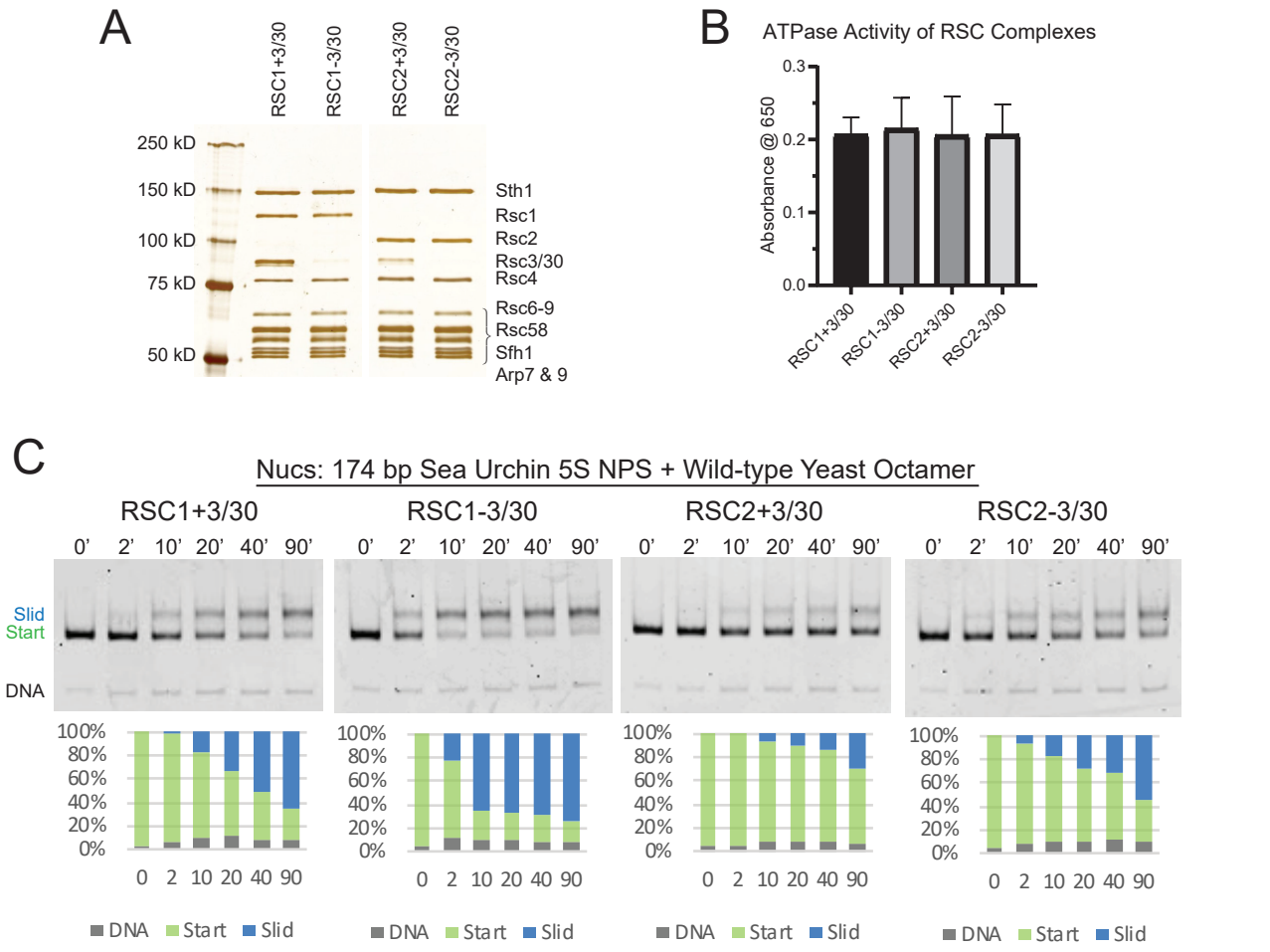

Figure 2. RSC1 and RSC2 complexes differ in remodeling activity on a sea urchin *5S* mononucleosomal substrate. (A) Alternative RSC1 and RSC2 complexes, with the Rsc3/30 module maintained or removed during purification. Purified RSC complexes (600 ng) were analyzed on 6% polyacrylamide SDS-PAGE gel stained with silver. The RSC1 and RSC2 complexes are from the same gel, but were moved adjacent for the depiction. (B) ATPase assay of RSC1 and RSC2 with and without the Rsc3/30 module. Values are the average +/- standard deviation from three separate RSC preps for each type of RSC assayed in duplicate. (C) Comparative sliding of 174 bp sea urchin *5S* yeast mononucleosomes (20 nM) by RSC1 and RSC2 complexes (30 nM). The nucleosomal Start (green), Slid (blue), and free DNA (grey) bands were quantified and reported as a percent of the total signal. Replicates (RSC1+3/30, 12x; RSC1-3/30, 9x; RSC2+3/30, 7x; RSC2-3/30, 11x) from two or more separate RSC preparations.

Figure 2 - figure supplement 1. RSC complexes without Rsc3/30 module are ATP-dependent chromatin remodelers and RSC1 and RSC2 complexes bind similarly to 174 bp sea urchin *5S* mononucleosomes.

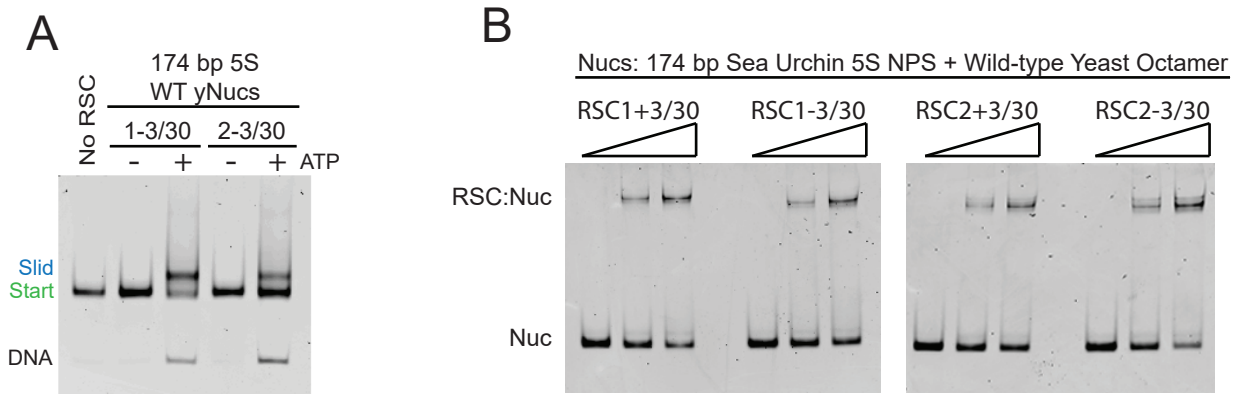

Figure 2 - figure supplement 1. RSC complexes without Rsc3/30 module are ATP-dependent chromatin remodelers and RSC1 and RSC2 complexes bind similarly to 174 bp sea urchin 5S mononucleosomes. (A) RSC1 and RSC2 complexes slide mononucleosomes in an ATP-dependent manner. Mononucleosomes (20 nM) were incubated in the presence (+) or absence (-) of 1 mM ATP with 30 nM of either the RSC1-3/30 (1-3/30) or the RSC2-3/30 (2-3/30) complex for 90 min at 30°C. Experiment conducted once. (B) RSC1 and RSC2 complexes bind similarly to mononucleosomes with 174 bp sea urchin *5S* DNA and wild-type yeast octamers. Nucleosomes (20 nM) were incubated with 0, 30, or 60 nM RSC for 20 min at 30˚C, run on a 3.8% native polyacrylamide gel, and stained with ethidium bromide. One of two or more technical replicates shown.

H3	1	2	3	4	5	6	7	8	9	10	11	12
A	R2A	T11A	L20A	T32A	R40A	R49A	S57A	L65A	E73A	L82A	L92A	V101A
B	T3A	G12A	S22A	G33A	Y41A	E50A	T58A	P66A	I74A	R83A	Q93A	S102A
C	K4A	G13A	K23A	G34A	K42A	I51A	E59A	F67A	Q76A	F84A	E94A	L103A
D	Q5A	K14A	R26A	V35A	P43A	R52A	L60A	Q68A	D77A	Q85A	S95A	F104A
E	T6A	P16A	K27A	K36A	G44A	R53A	L61A	R69A	F78A	S86A	V96A	E105A
F	R8A	R17A	S28A	K37A	T45A	F54A	I62A	L70A	K79A	S87A	E97A	D106A
G	K9A	K18A	P30A	P38A	V46A	Q55A	R63A	V71A	T80A	I89A	Y99A	T107A
H	S10A	Q19A	S31A	H39A	L48A	K56A	K64A	R72A	D81A	G90A	L100A	N108A
H3	1	2	3	4	5	6	7	8	9	10	11	12
A	L109A	Q120A	R129A									
B	I112A	K121A	L130A									
C	H113A	K122A	R131A									
D	K115A	D123A	G132A									
E	R116A	I124A	E133A									
F	V117A	K125A	R134A									
G	T118A	L126A	S135A									
H	I119A	R128A										
H4	1	2	3	4	5	6	7	8	9	10	11	12
A	S1A	G9A	H18A	I26A	R35A	K44A	E52A	F61A	S69A	R78A	V86A	R95A
B	G2A	L10A	R19A	Q27A	R36A	R45A	E53A	L62A	V70A	K79A	V87A	T96A
C	R3A	G11A	K20A	G28A	L37A	I46A	V54A	E63A	T71A	T80A	Y88A	L97A
D	G4A	K12A	I21A	I29A	R39A	S47A	R55A	S64A	Y72A	V81A	L90A	Y98A
E	K5A	G13A	L22A	T30A	R40A	G48A	V57A	V65A	T73A	T82A	K91A	G99A
F	G6A	G14A	R23A	K31A	G41A	L49A	L58A	I66A	E74A	S83A	R92A	F100A
G	G7A	K16A	D24A	P32A	G42A	I50A	K59A	R67A	H75A	L84A	Q93A	G101A
H	K8A	R17A	N25A	I34A	V43A	Y51A	S60A	D68A	K77A	D85A	G94A	G102A

Lethal w/ rsc1Δ | *Lethal w/ rsc2Δ* | *Lethal w/ rsc1Δ and rsc2Δ* | *Lethal in WT*

Table 1: Summary of Histone H3-H4 screen with *rsc1*Δ and *rsc2*Δ. Library of *TRP1*-marked plasmids containing H3-H4 residues mutated to alanine were transformed into *h3-h4*Δ [*H3-H4.URA3*] (YBC1939), *rsc1*Δ *h3-h4*Δ [*H3-H4.URA3*] (YBC2090) or *rsc2*Δ *h3-h4*Δ [*H3-H4.URA3*] (YBC3040), and spotted to SC-TRP, or SC-TRP+5FOA to force the loss of the wild type (WT) histone plasmid and test for synthetic lethality. Histone mutations that were lethal on their own in WT RSC are shaded grey, those that were lethal in combination with *rsc1*Δ are highlighted yellow, those that were lethal with *rsc2*Δ are highlighted in blue, and those residues that were lethal with *rsc1*Δ as well as with *rsc2*Δ are highlighted in green. Histone screen was performed one time and plasmids from lethal mutations were isolated and retransformed. Two or more transformants were tested to confirm phenotype.

Mutation	* FRET %	Phenotype
WT	100 ± 6	No phenotype
R40A	71 ± 7	Lethal w/ *rsc1*Δ
Y41A	72 ± 7	Lethal w/ WT
K42A	54 ± 3	Lethal w/ *rsc1*Δ
P43A	91 ± 3	No phenotype
G44A	68 ± 9	Lethal w/ *rsc1*Δ
T45A	52 ± 5	Lethal w/ WT
V46A	89 ± 5	Lethal w/ *rsc1*Δ
L48A	86 ± 4	Lethal w/ WT
R49A	67 ± 3	Lethal w/ *rsc1*Δ
E50A	98 ± 6	No phenotype
I51A	81 ± 13	Lethal w/ WT
R52A	78 ± 3	Lethal w/ *rsc1*Δ
R53A	80 ± 4	No phenotype
F54A	96 ± 3	Lethal w/ WT
Q55A	69 ± 11	Lethal w/ WT
K56A	95 ± 4	No phenotype
S57A	102 ± 5	No phenotype
K56Q	82 ± 2	Lethal w/ *rsc1*Δ

* DNA end to end FRET,
from Ferreira et al, 2007

Table 1- table supplement 1. DNA end to end FRET measurements on mononucleosomes containing H3 αN helix mutations from Ferreira et al, 2007 with the phenotype when combined with *RSC*, *rsc1Δ,* or *rsc2Δ*.

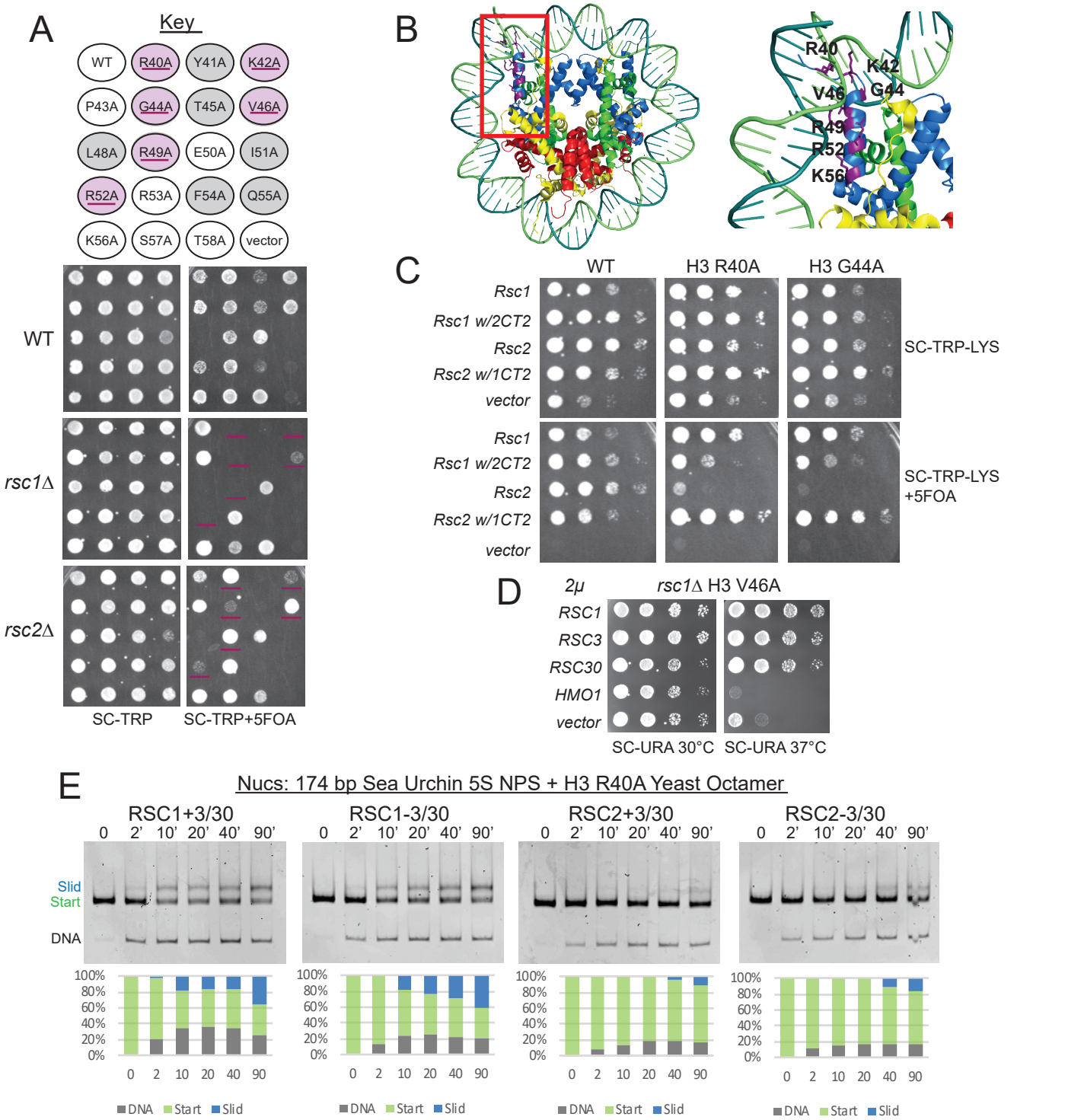

Figure 3. Mutations in the H3 αN helix are lethal in combination with r*sc1Δ,* but not *rsc2Δ*, and they reduce RSC remodeling of the *5S* nucleosome. (A) Histone H3 αN helix mutations that are lethal with *rsc1Δ*. *TRP1*-marked plasmids containing WT H4, and H3 mutations within the αN helix were transformed into *h3-h4Δ* [*H3-H4.URA3*] (YBC1939), *rsc1Δ h3-h4Δ* [*H3-H4.URA3*] (YBC2090) or *rsc2Δ h3-h4Δ* [*H3-H4.URA3*] (YBC3040), and spotted to SC-TRP or SC-TRP+5FOA to enforce the loss of the WT histone plasmid. Mutations that were lethal on their own without mutated RSC are shaded in grey. Mutations that were lethal in *rsc1Δ* but not *rsc2Δ* are shaded in purple and underlined. Transformants were grown at 30°C for 2 days. Shown is one of two biological replicates. (B) Location of the synthetic lethal *rsc1Δ* H3 αN helix mutations are depicted in purple on the nucleosome, PDB code 5NL0. (C) The *RSC1 CT2* region complements the synthetic lethal *rsc1Δ* H3 αN helix mutations. *rsc1Δ rsc2Δ h3-h4Δ* [*RSC1.URA3*] with [*H3.WT*, *R40A*, or *G44A-H4.WT. LYS2*] (YBC3466, YBC3444, YBC3433) transformed with *TRP1*-marked plasmids bearing *RSC1* (p609), *RSC2* (p604), *RSC1 w/2CT2* (p3097), *RSC2 w/1CT2* (p3098), or vector (pRS314) and spotted as 10x serial dilution to SC-TRP-LYS, or SC-TRP-LYS+5FOA. Shown is one of four biological replicates. (D) High-copy *RSC3* or *RSC30* will partially suppress the Ts⁻ phenotype of *rsc1Δ* H3V46A. Strain *rsc1Δ h3-h4Δ* [*H3.V46A-H4.WT.TRP*] (YBC3586) transformed with *URA3*-marked high copy (*2μ*) plasmids containing *RSC1* (p705), *RSC3* (p1310), *RSC30* (p916), *HMO1* (p3390), or vector (pRS426), and spotted as 10x serial dilutions at 30°C or 37°C. Shown is one of two biological replicates. (E) Comparative sliding and ejection of 174 bp sea urchin *5S* NPS H3 R40A yeast mononucleosomes (20 nM) by RSC1 and RSC2 complexes (30 nM). The nucleosomal Start (green), Slid (blue), and free DNA (grey) bands were quantified and reported as a percent of the total signal. Replicates (RSC1+3/30, 5x; RSC1-3/30, 3x; RSC2+3/30, 4x; RSC2-3/30, 4x) from two separate RSC preparations.

Figure 3 - figure supplement 1. Complementation by CT2 domain swaps when combined with H3 αN helix mutations.

Figure 3 - figure supplement 2. RSC1 and RSC2 complexes bind similarly to 174 bp sea urchin *5S* yeast mononucleosomes with the H3 R40A mutation.

Figure 3 - figure supplement 3. Mapping the positions of the wt and H3 R40A 174 bp sea urchin *5S* yeast mononucleosomes.

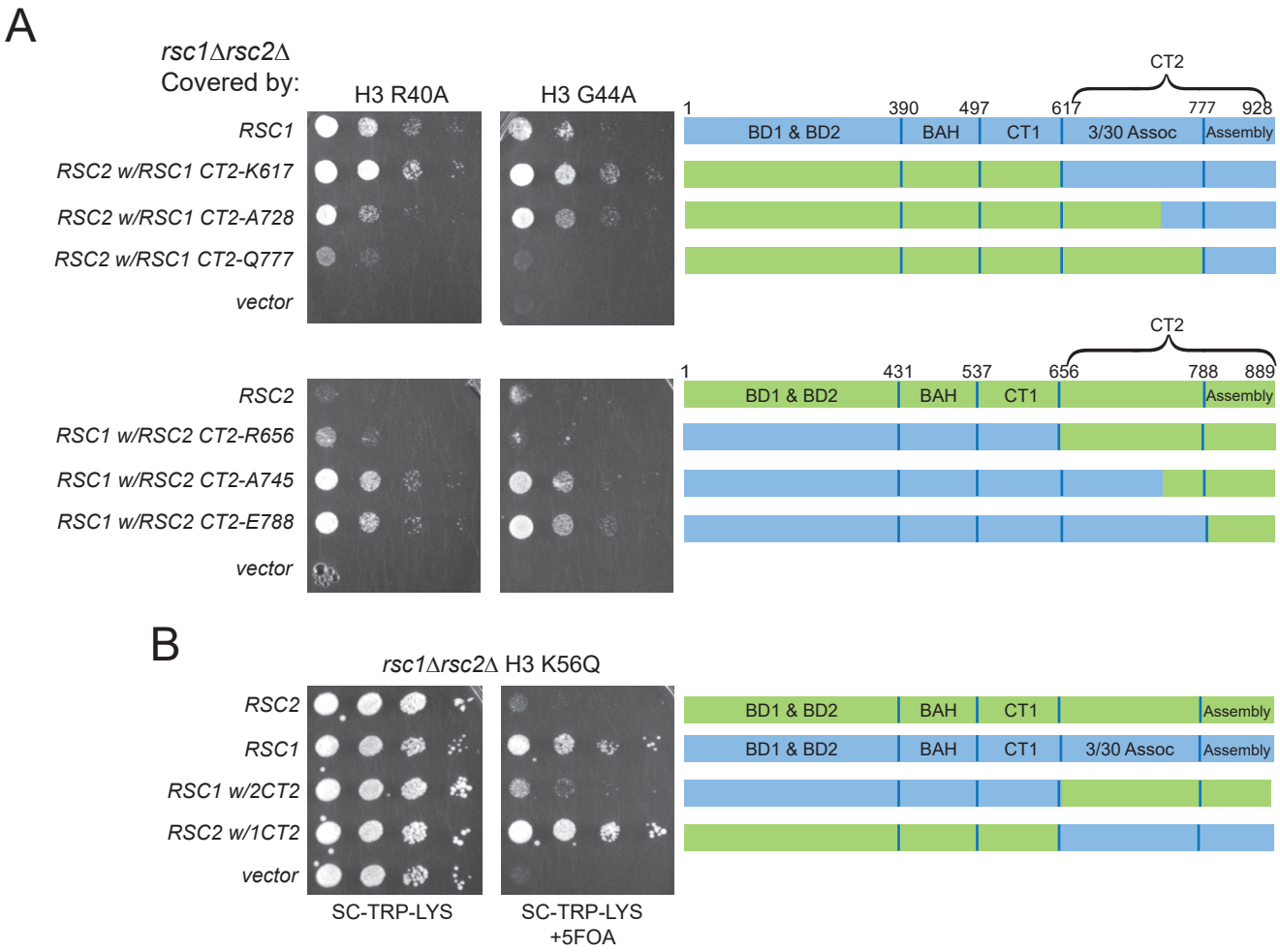

Figure 3 - figure supplement 1. Complementation by CT2 domain swaps when combined with H3 αN helix mutations. (A) The *RSC1 CT2* region complements the synthetic lethal *rsc1*Δ H3 αN helix mutations. Strain *rsc1*Δ *rsc2*Δ *h3-h4*Δ [*RSC1.URA3*] [*H3. R40A*, or *G44A-H4.WT. LYS2*] (YBC3444, YBC3433) transformed with *TRP1*-marked plasmids bearing *RSC1* (p609), *RSC2* (p604), C-Terminal swaps at positions noted (p3098, p3165, p3167, p3097, p3166, p3164) or vector (pRS314) and spotted as 10x serial dilution to SC-TRP-LYS, or SC-TRP-LYS+5FOA. One of four biological replicates shown. (B) Synthetic lethality of *rsc1*Δ H3 K56Q is complemented by the *RSC1 CT2* region. Strain *rsc1*Δ *rsc2*Δ *h3-h4*Δ [*RSC1.URA3*] [*H3.K56Q-H4.WT. LYS2*] (YBC3432) transformed with *TRP1*-marked plasmids bearing *RSC1* (p609), *RSC2* (p604), *RSC1 w/2CT2* (p3097), *RSC2 w/1CT2* (p3098), or vector (pRS314) and spotted as 10x serial dilution to SC-TRP-LYS, or SC-TRP-LYS+5FOA. One of four biological replicates shown.

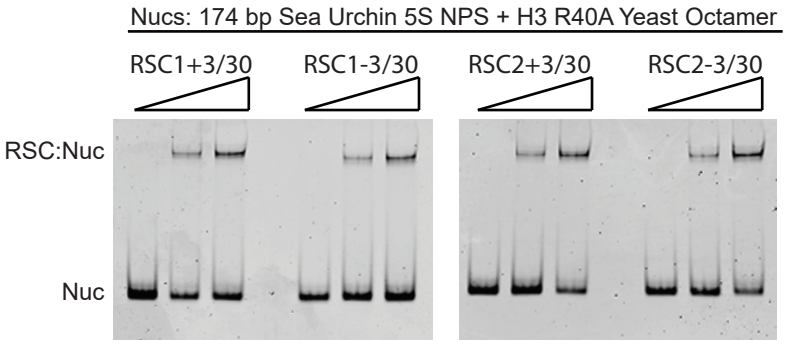

Figure 3 - figure supplement 2. RSC1 and RSC2 complexes bind similarly to 174 bp sea urchin *5S* yeast mononucleosomes with the H3 R40A mutation. Nucleosomes (20 nM) were incubated with 0, 30, or 60 nM RSC for 20 min at 30°C, run on a 3.8% native polyacrylamide gel, and stained with ethidium bromide. One of two or more technical replicates shown.

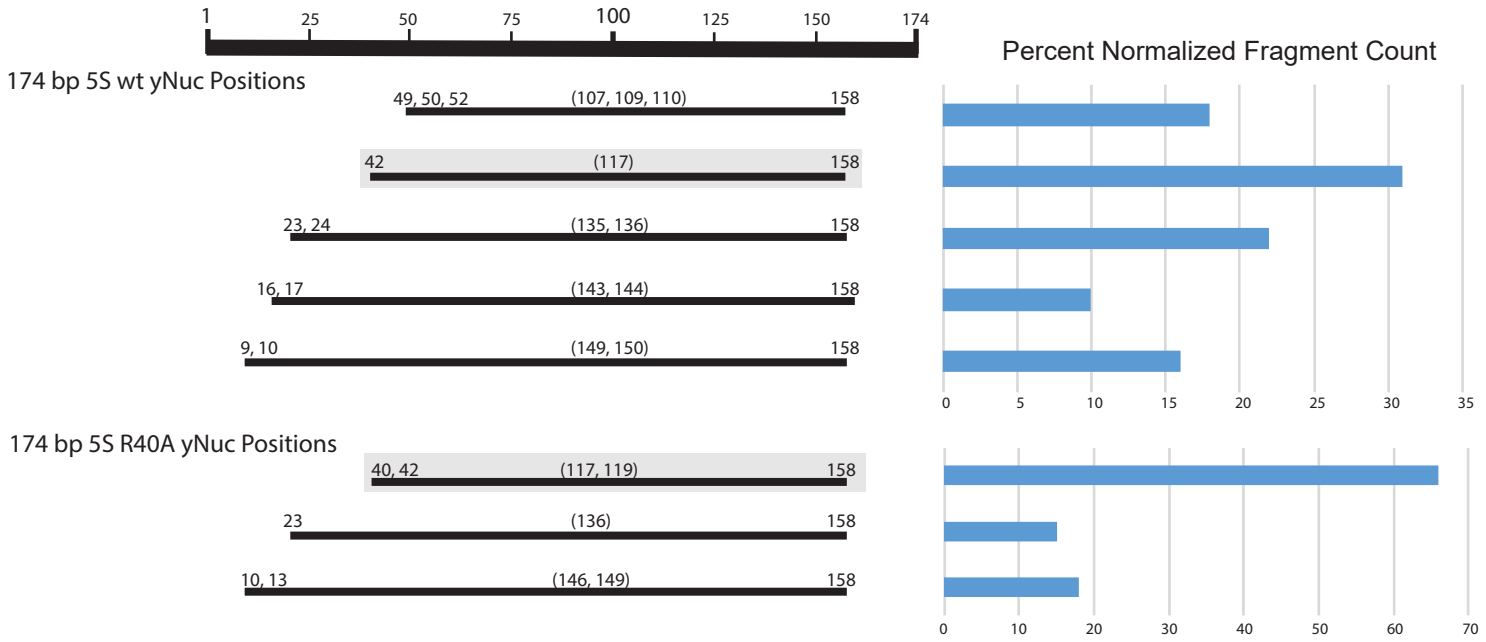

Figure 3 - figure supplement 3. Mapping the positions of the wt and H3 R40A 174 bp sea urchin *5S* yeast mononucleosomes. Nucleosome mapping by ExoIII and S1 treatment followed by next-generation sequencing. Experiment conducted once.
Figure 3 - figure supplement 3 - Source Data 1. 174 bp *5S* nucleosome mapping.

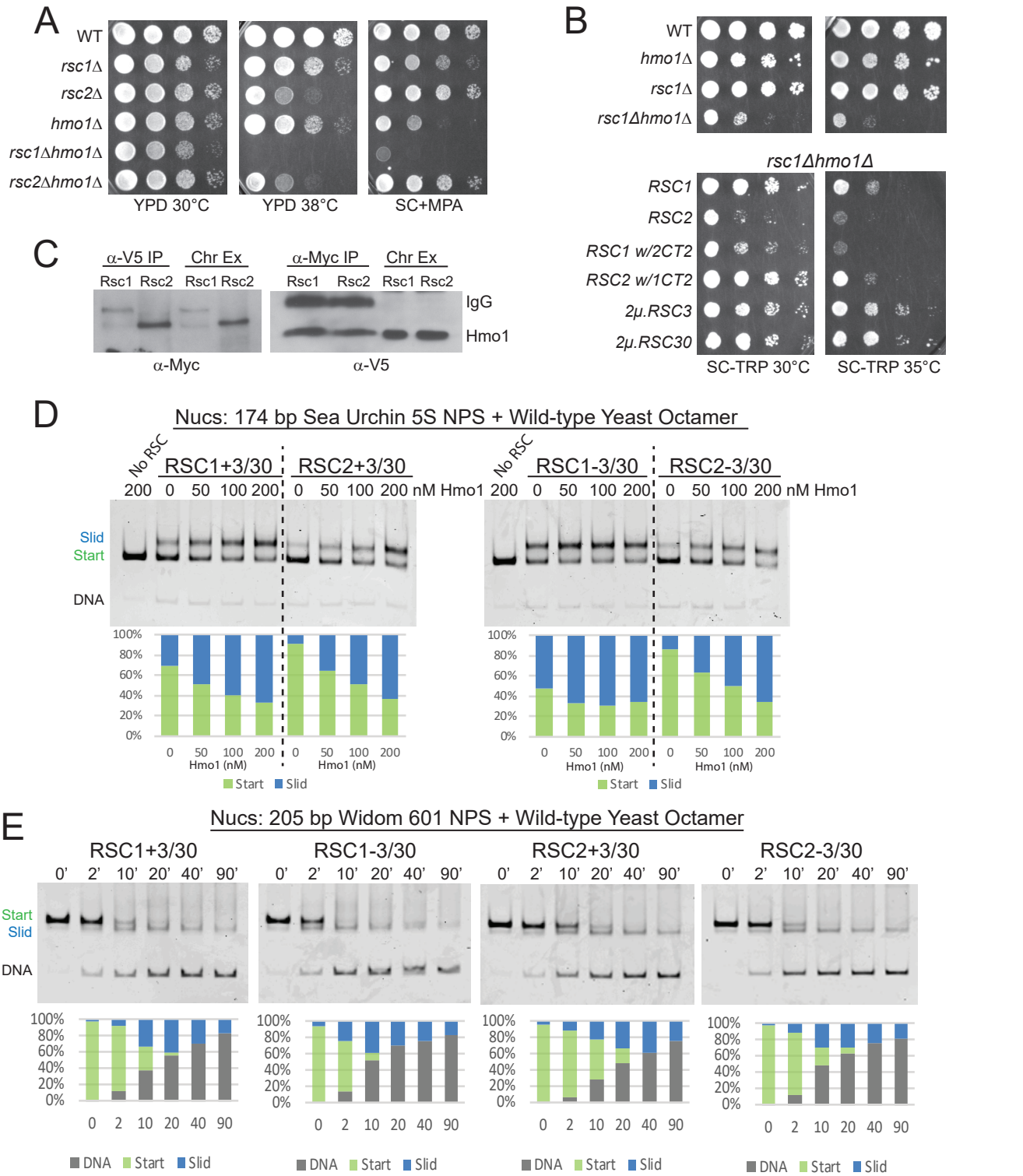

Figure 4. Hmo1 cooperates with RSC to remodel fragile or partially-unwrapped nucleosomes. (A) An *hmo1* null mutation is synthetically sick with *rsc1*Δ, but not *rsc2*Δ. WT (YBC604), *rsc1*Δ (YBC774), *rsc2*Δ (YBC82), *hmo1*Δ (YBC3509), *rsc1*Δ (YBC774), *rsc2*Δ (YBC82), *rsc1*Δ *hmo1*Δ (YBC3514), *rsc2*Δ *hmo1*Δ (YBC3515) spotted as 10x serial dilutions to YPD 30°C, YPD 38°C, and SC+20 μg/ml mycophenolic acid (MPA). One of two or more biological replicates shown. (B) The *rsc1*Δ *hmo1*Δ synthetic sickness is suppressed by high copy *RSC3*, *RSC30*, or *RSC1 CT2*. Strain *rsc1*Δ *hmo1*Δ (YBC3514) transformed with *TRP1*-marked *RSC1* (p609), *RSC2* (p604), *RSC1 w/2CT2* (p3097), *RSC2 w/1CT2* (p3098), *2μ.RSC3* (p929), *2μ.RSC30* (p911), or vector (pRS314) spotted as 10x serial dilutions to SC-TRP 30°C or SC-TRP 35°C. One of four biological replicates shown. (C) Co-IP of Rsc1 and Rsc2 with Hmo1. Sonicated chromatin extracts from *RSC1.9XMYC HMO1.V5* (YBC3558) and *RSC2.9XMYC HMO1.V5* (YBC3559) were immunoprecipitated using anti-Myc or anti-V5. Western blots were probed with anti-Myc or anti-V5 antibodies. One of three biological replicates shown. (D) Comparative sliding by RSC1 and RSC2 complexes (10 nM) of 174 bp sea urchin *5S* yeast mononucleosomes (20 nM) pre-incubated with increasing concentrations of Hmo1 protein. Reactions were conducted at 30°C for 20 min. The Start (green) and Slid (blue) bands were quantified and reported as percent of the total signal. The free DNA band was negligible and not quantified. One of 3 technical replicates shown. (E) Comparative sliding and ejection of Widom 601 yeast mononucleosomes (20 nM) by RSC1 and RSC2 complexes (10 nM). The nucleosomal Start (green), Slid (blue), and free DNA (grey) bands were quantified and reported as a percent of the total signal. Replicates (RSC1+3/30, 7x; RSC1-3/30, 3x; RSC2+3/30, 4x; RSC2-3/30, 7x) from two or more separate RSC preparations.

Figure 4 - figure supplement 1. Additional sliding assays of 174 bp *5S* yeast mononucleosomes with RSC and Hmo1.

Figure 4 - figure supplement 2. RSC1 and RSC2 slide Widom 601 H3 R40A mononucleosomes similarly.

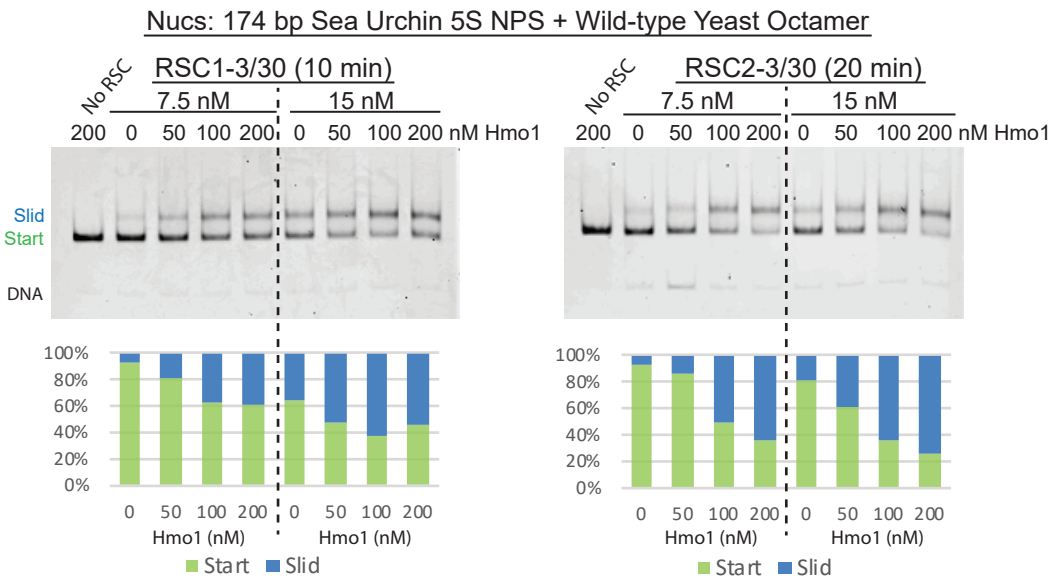

Figure 4 - figure supplement 1. Additional sliding assays of 174 bp *5S* yeast mononucleosomes with RSC and Hmo1. 174 bp *5S* yeast mononucleosomes (20 nM) were pre-incubated with increasing concentrations of Hmo1. RSC concentrations and reaction times are as indicated. All reactions were conducted at 30°C. The Start (green) and Slid (blue) bands were quantified and reported as percent of the total signal. The free DNA band was negligible and not quantified. One of two technical replicates shown.

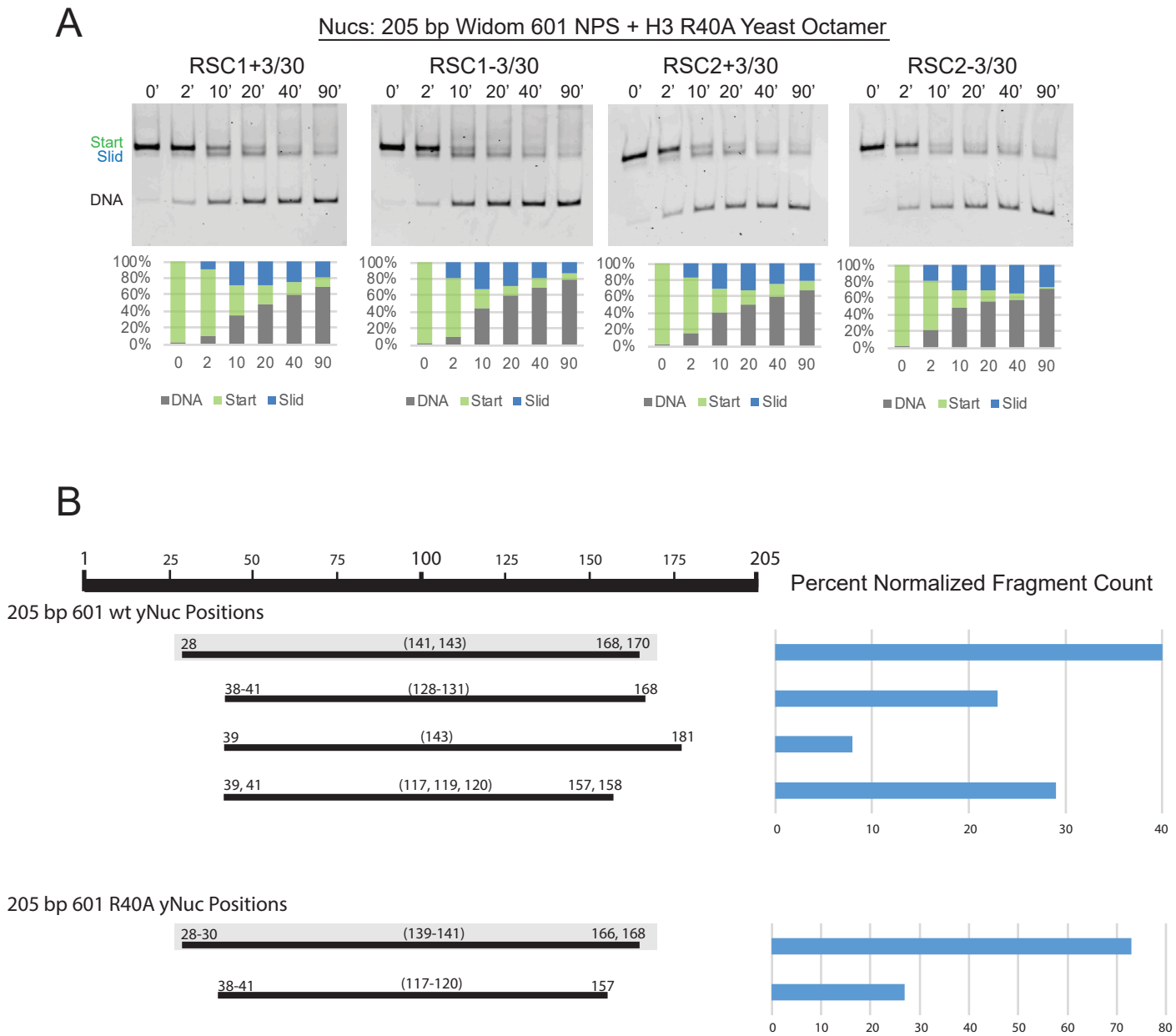

Figure 4 - figure supplement 2. RSC1 and RSC2 slide Widom 601 H3 R40A mononucleosomes similarly. (A) Comparative sliding of RSC1 and RSC2 complexes (10 nM) on H3 R40A 205 bp Widom 601 yeast mononucleosomes (20 nM). The nucleosomal Start (green), Slid (blue), and free DNA (grey) bands were quantified and reported as a percent of the total signal. Replicates (RSC1+3/30, 6x; RSC1-3/30, 3x; RSC2+3/30, 3x; RSC2-3/30, 5x) from two or more separate RSC preparations. (B) Mapping the positions of the wild-type and H3 R40A 205 bp Widom 601 yeast mononucleosomes by ExoIII and S1 treatment as in Figure 3 -figure supplement 3. Averages from two technical replicates.
Figure 4 - figure supplement 2 - Source Data 1. 205 bp Widom 601 nucleosome mapping.

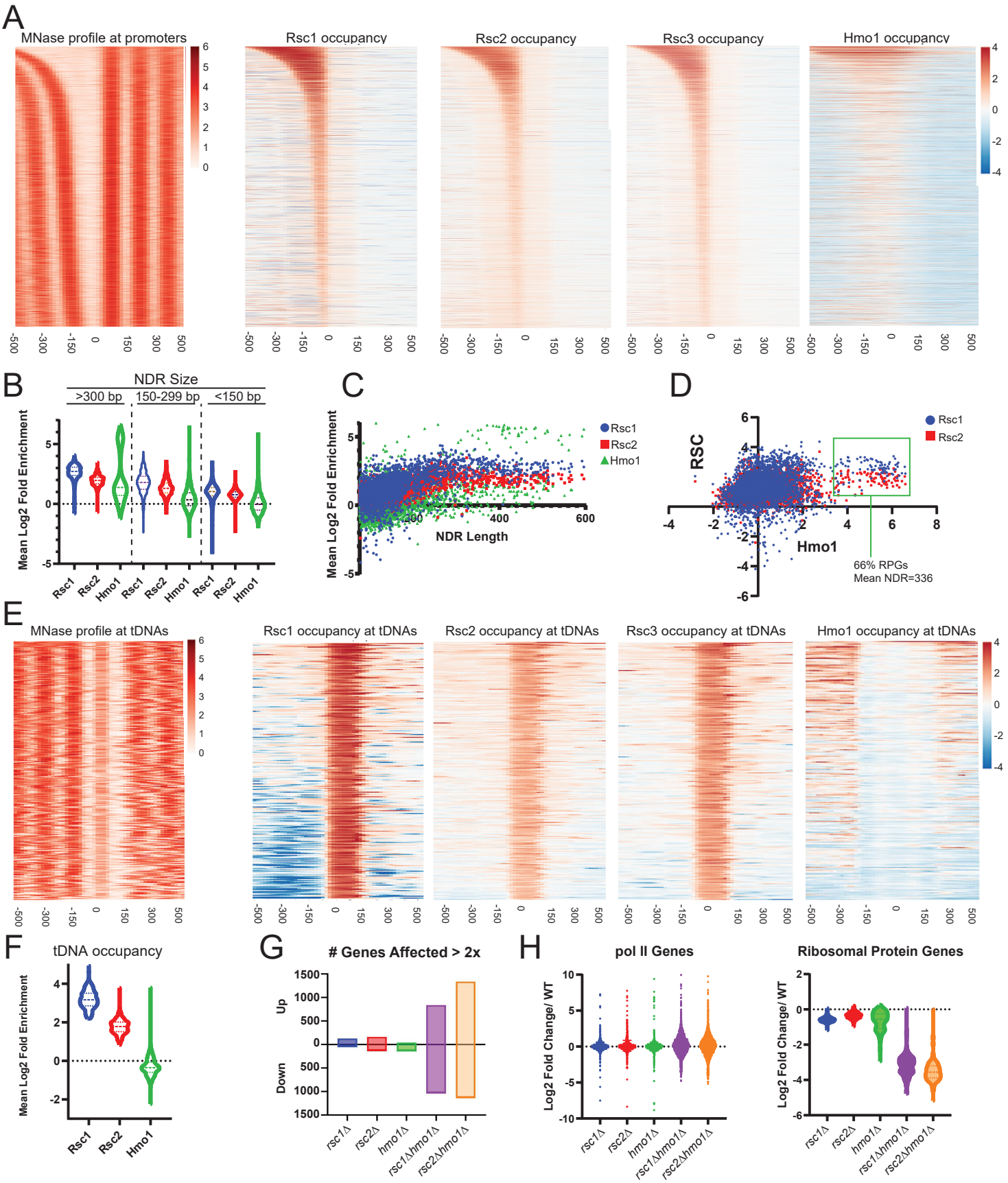

Figure 5. Rsc1 and Rsc2 occupy promoters with wide NDRS, with preferential occupancy of RSC1 at tDNAs. (A) Heat maps showing enrichment of nucleosomes, Rsc1, Rsc2, Rsc3, and Hmo1 at promoters, sorted by NDR length. (B) Violin plot of Rsc1, Rsc2, and Hmo1 occupancy at promoters at three categories of NDR length. (C) Plot of Rsc1, Rsc2, and Hmo1 occupancy compared to NDR length. (D) Plot of Rsc1 and Rsc2 enrichment by Hmo1 occupancy. (E) Heat maps showing enrichment of nucleosomes, Rsc1, Rsc2, Rsc3, and Hmo1 at all tDNAs (tRNA encoding genes). (F) Violin plot of Rsc1, Rsc2, and Hmo1 mean log2 fold enrichment at tDNAs. (G) Number of genes affected by *rsc* and *hmo1* deletions. For each mutation the number of genes up or downregulated two fold or more compared to WT, adjusted p value <0.05, *rsc1*Δ (↑129↓45), *rsc2*Δ (↑160↓129), *hmo1*Δ (↑44↓132), *rsc1*Δ*hmo1*Δ (↑838↓1028), *rsc2*Δ*hmo1*Δ (↑1336↓1131). (H) Gene Expression changes. Violin plots of RNA expression for each mutation at all pol II genes (6145 genes) and at ribosomal protein genes (132 genes) as compared to WT expression. ChIPSeq and RNASeq data shown represents averages of two and three biological replicates, respectively.

Figure 5 - figure supplement 1. Gene expression changes in *rsc1*Δ, *rsc2*Δ, and *hmo1*Δ mutants.

Figure 5 - figure supplement 2. Gene expression changes in *rsc1*Δ, *rsc2*Δ, and *rsc30*Δ mutants.

Figure 5 - figure supplement 3. Appearance of *RSC1/RSC2*, *RSC3/RSC30*, and *HMO1* in yeast evolution.

Figure 5 - Source Data 1-3. Occupancy and differential expression of RSC subunits and mutants.

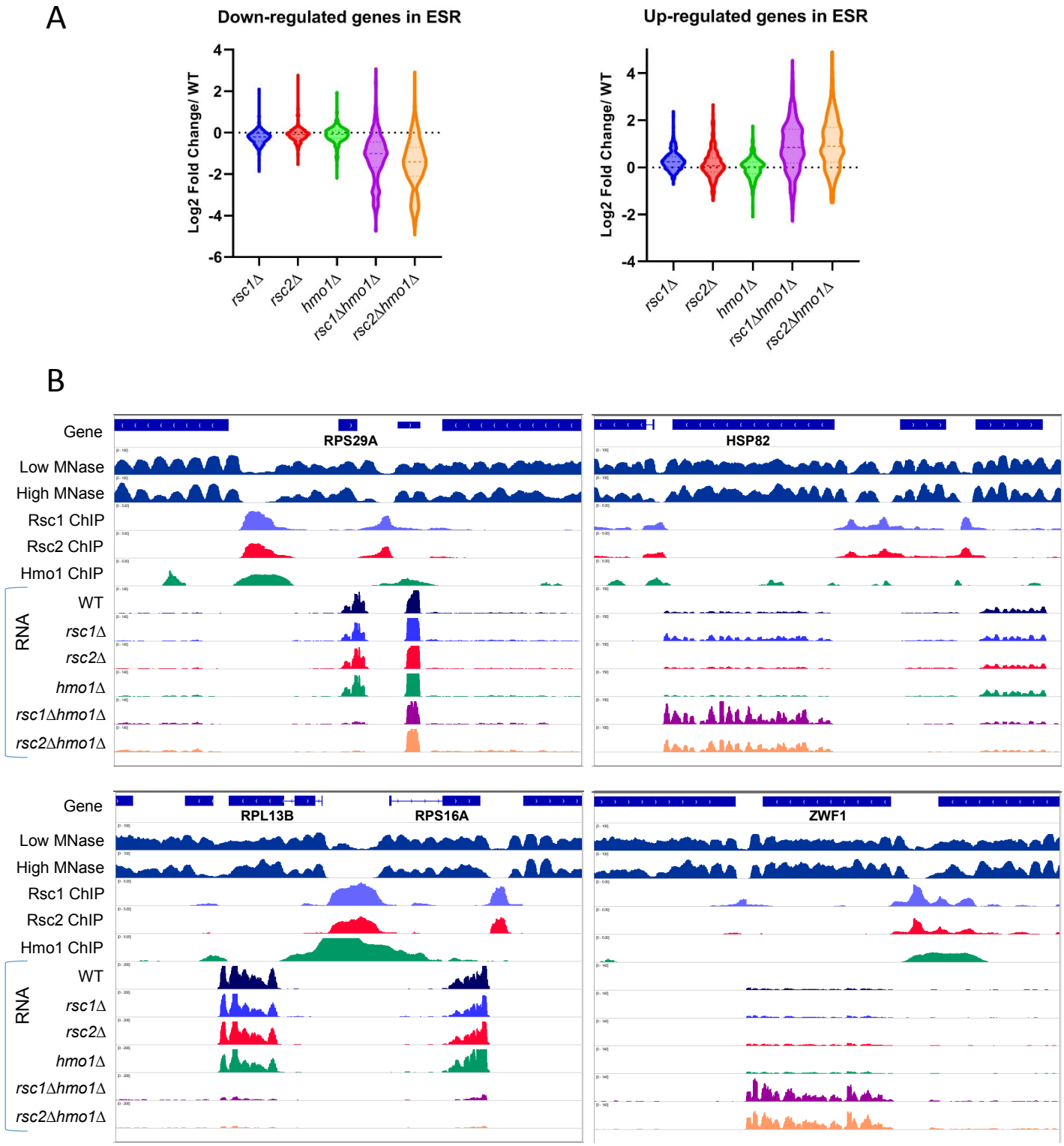

Figure 5- figure supplement 1. Gene expression changes in *rsc1*Δ, *rsc2*Δ, and *hmo1*Δ mutants.
(A) The effect of *rsc* deletions on genes involved in the environmental stress response (ESR). Violin plot showing expression changes (average of three biological replicates) in *rsc* mutants for genes that are up-regulated (255 genes) or down regulated (587 genes) in the ESR (Gasch et al, 2000). (B) Genome Snapshots. Shown for select genes are low- (GSM1891202) and high- (GSM1891207) MNase digested fragment coverage from Kubik et al, 2015, Rsc1 and Rsc2 ChIP Seq log2 fold enrichments, Hmo1 ChIP Seq log2 fold enrichment (GSM1509041) from Knight et al, 2014, RNASeq coverage (unstranded) from one of three biological replicates of RNAseq for WT(YBC604), *rsc1*Δ (YBC774), *rsc2*Δ (YBC82), *hmo1*Δ (YBC3509), *rsc1*Δ *hmo1*Δ (YBC3514), *rsc2*Δ *hmo1*Δ (YBC3515).
Figure 5- figure supplement 1- Source Data 1. List of ESR affected genes.

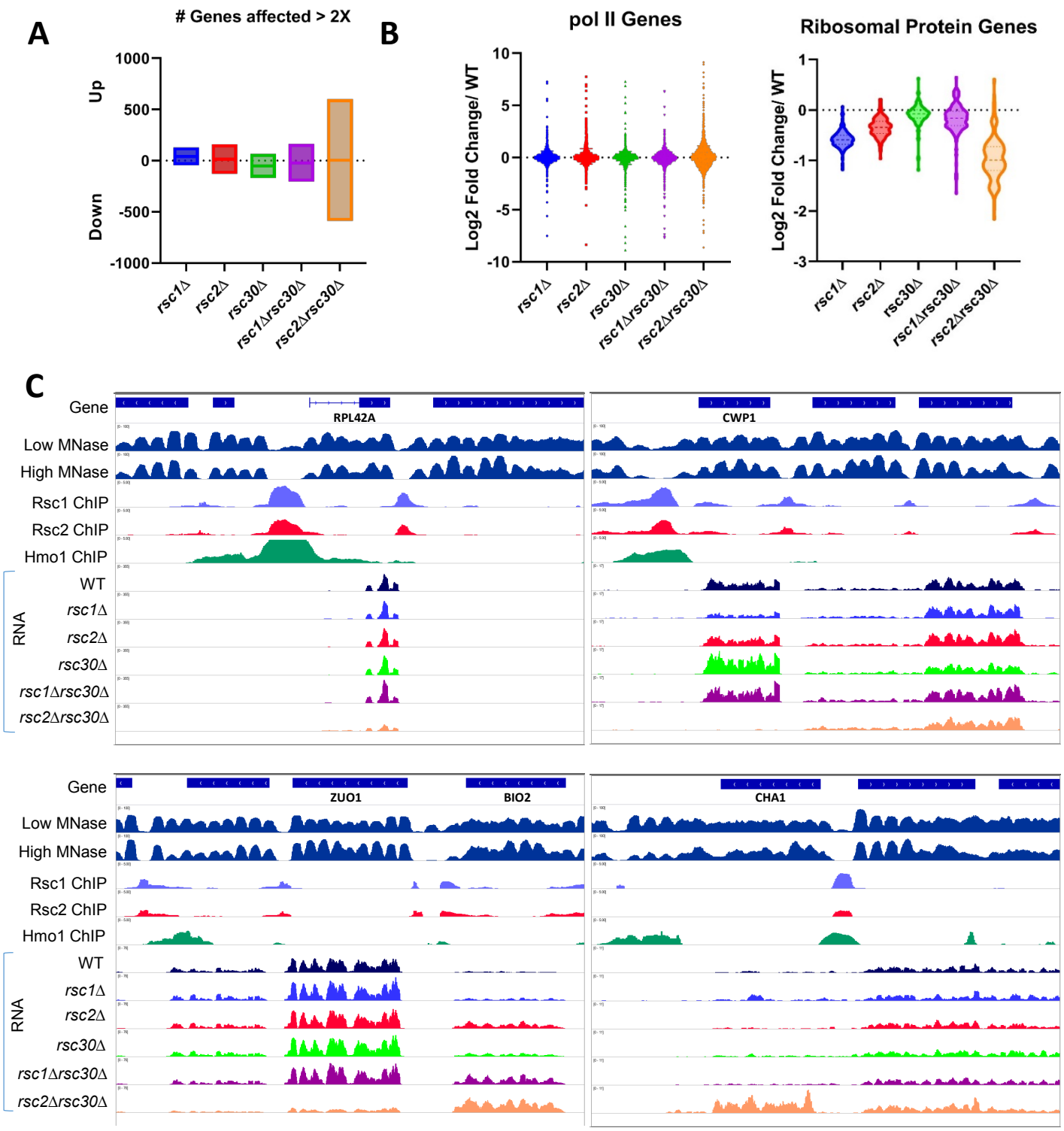

Figure 5 – figure supplement 2: Gene expression changes in *rsc1*Δ, *rsc2*Δ, and *rsc30*Δ mutants. (A) Number of genes affected by *rsc* deletions. For each mutation, the number of genes up or downregulated two fold or more compared to WT. *rsc1*Δ (↑129↓45), *rsc2*Δ (↑160↓129), *rsc30*Δ (↑66↓168), *rsc1*Δ*rsc30*Δ (↑162↓204), *rsc2*Δ*rsc30*Δ (↑601↓589). (B) Gene Expression changes. Violin plots showing log2 fold change of RNA in mutants at all pol II genes (6145 genes) and at ribosomal protein genes (132 genes) compared to WT expression. Change in expression reflects an average of three biological replicates, Figure 5- Source Data 3. (C) Genome snapshots. Shown for select genes are low- (GSM1891202) and high- (GSM1891207) MNase-digested fragment coverage from Kubik et al, 2015, Rsc1 and Rsc2 ChIP seq log2 fold enrichments, Hmo1 ChIP Seq log2 fold enrichments (GSM1509041) from Knight et al, 2014, and RNASeq coverage (unstranded) from one of three replicates of RNAseq for WT (YBC604), *rsc1*Δ (YBC774), *rsc2*Δ (YBC82), *rsc30*Δ (YBC695), *rsc1*Δ *rsc30*Δ (YBC839), and *rsc2*Δ *rsc30*Δ (YBC910).

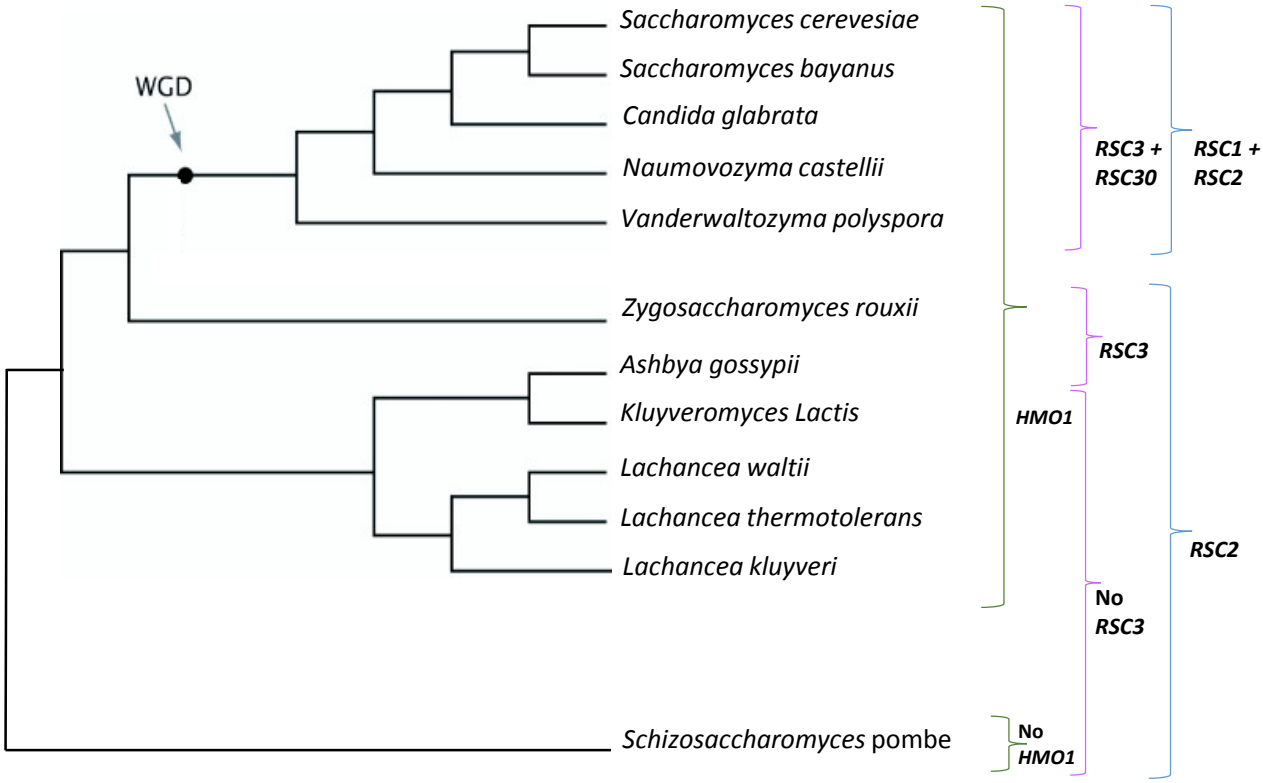

Figure 5- supplement 3. Appearance of *RSC1/RSC2*, *RSC3/RSC30*, and *HMO1* in yeast evolution. Phylogenetic tree adapted from OhÉigeartaigh et al, 2011 with the appearance of *RSC1/RSC2*, *RSC3/RSC30*, and *HMO1* as determined by NCBI Fungal BLAST **(Figure 5- table supplement 1).** WGD refers to whole genome duplication. Duplication of *RSC2* and *RSC3* resulted in *RSC1* and *RSC30* in *S. cerevisiae*. While the duplicated genes in other organisms may still more closely resemble *RSC2* or *RSC3*, *RSC1* and *RSC30* have been used to indicate the duplicated copy.

Yeast Species	Rsc1/2 ortholog protein identifier	Rsc2 score	Rsc2 E value	Rsc1 score	Rsc1 E value
Candida glabrata *	CAG57994.1	794	0	637	0
Candida glabrata *	CAG61377.1	695	0	762	0
Naumovozyma castelii *	XP_003673169.1	788	0	698	0
Naumovozyma castelii *	XP_003678436.1	704	0	651	0
Vanderwaltozyma polyspora *	XP_001643414.1	718	0	770	0
Vanderwaltozyma polyspora *	XP_001643343.1	621	0	583	0
Zygosaccharomyces rouxii	ZYRO0B07986p	875	0	805	0
Ashbya gossypii	ABL005Cp	751	0	687	0
Lachancea thermotolerans	XP_002551602.1	785	0	711	0
Kluyveromyces lactis	CAH025113.1	501	2E-163	506	8E-165
Candida albicans	EEQ42885.1	405	3E-128	398	4E-125
Yarrowia lipolytica	XP_503084.1	316	5E-95	288	2E-84
Schizosaccharomyces pombe	CAA19283.1	224	1E-62	223	4E-62

Yeast Species	Rsc3/30 ortholog protein identifier	Rsc3 score	Rsc3 E value	Rsc30 score	Rsc30 E value
Candida glabrata *	CAG59797.1	389	5E-123	113	3E-36
Candida glabrata *	CAG58494.1	149	2E-37	100	4E-22
Naumovozyma castelii *	XP_003677109.1	532	2E-177	143	1E-35
Naumovozyma castelii *	XP_003673610.1	75.1	2E-14	77.8	4E-15
Vanderwaltozyma polyspora *	XP_001646730.1	495	2E-163	103	3e-323
Vanderwaltozyma polyspora *	XP_001642773.1	358	4E-111	119	5E-28
Zygosaccharomyces rouxii	ZYRO0C13882p	577	0	127	2E-30
Ashbya gossypii	AAL057Cp	400	1E-126	97.1	7E-21
Lachancea thermotolerans	No significant ortholog				
Kluyveromyces lactis					
Candida albicans					
Yarrowia lipolytica					
Schizosaccharomyces pombe					

Figure 5- table supplement 1. Alignment scores from NCBI Fungal Blast for Rsc1/Rsc2 and Rsc3/Rsc30 orthologs as compared to Rsc1, Rsc2, Rsc3, Rsc30 in *Saccharomyces cerevisiae* . Asterisk (*) denotes yeast species that arose after the whole genome duplication (WGD) event.

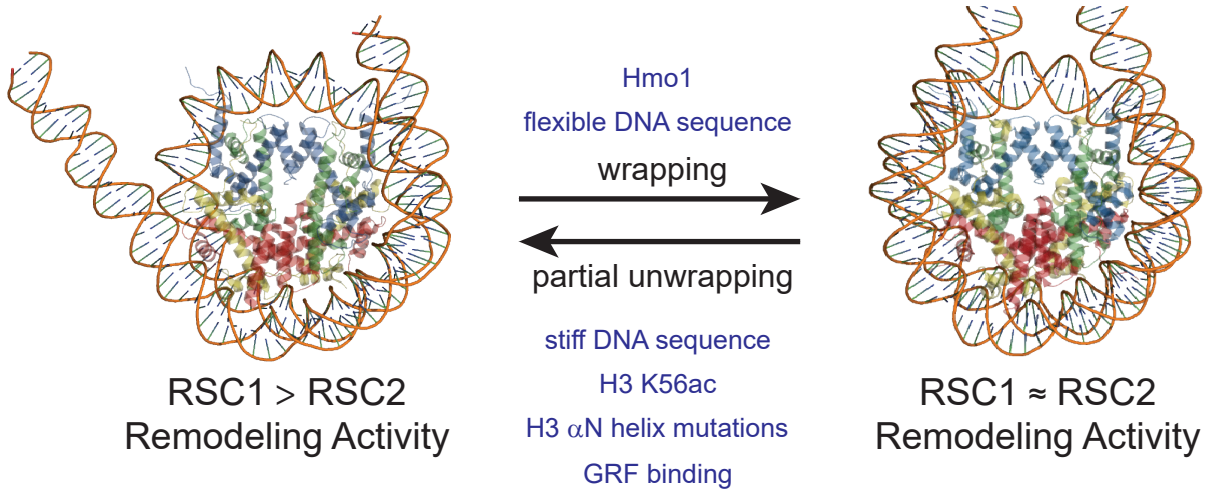

Figure 6. Model for RSC1 and RSC2 action on wrapped versus partially-unwrapped nucleosomes. Here, flexible/positioning DNA sequences and the protein Hmo1 promote wrapping (Anderson et al. 2002, Iyer 2012, Panday and Grove 2017). In contrast, partial unwrapping can be facilitated by 'stiff' (AT-rich) DNA sequences, acetylation (e.g. H3 K56ac), the binding of general regulatory transcription factors (not shown) to entry/exit DNA, or by mutation of residues within/near the H3 αN helix (which normally binds entry/exit DNA) (Segal and Widom 2009, Neumann et al. 2009, Knight et al. 2014, Ferreira et al. 2007). Whereas fully-wrapped nucleosomes are remodeled well by RSC1 or RSC2 complexes, partially-unwrapped nucleosomes are better managed and remodeled by RSC1 complexes.